Filtered Wrinkled Flamelets model for Large-Eddy Simulation of turbulent premixed combustion

Renaud Mercier, Cédric Mehl, Benoit Fiorina, Vincent Moureau

Filtered Wrinkled Flamelets model for Large-Eddy Simulation of turbulent premixed combustion

Renaud Mercier[a,*], Cédric Mehl[b], Benoît Fiorina[b], Vincent Moureau[c]

[a] Safran Tech, Modelling and Simulation, Rue des Jeunes Bois, Châteaufort, Magny-Les-Hameaux 78114, France
[b] Laboratoire EM2C, CNRS, CentraleSupélec, Université Paris-Saclay, 3 rue Joliot Curie, Gif-sur-Yvette 91190, France
[c] CORIA- CNRS UMR 6614-Normandie Université - Université et INSA de Rouen, Campus Universitaire du Madrillet, Saint Etienne du Rouvray, Rouen 76800, France

ARTICLE INFO

Article history:
Received 3 October 2017
Revised 12 December 2017
Accepted 18 March 2019
Available online 5 April 2019

Keywords:
Turbulent combustion
Premixed flames
Flame wrinkling
Filtered Wrinkled Flame
Large Eddy Simulation

ABSTRACT

Models for combustion LES based on a geometrical description of the reactive layer are well suited to capture the turbulent flame front displacement speed, but do not predict the filtered chemical flame structure. This article aims to discuss and model the impact of the flame sub-filter wrinkling level on the species production, with a focus on carbon monoxide emission. For that purpose, 2-D wrinkled flames with a sinusoidal pattern, which include detailed chemistry effects, are manufactured. Three controlling parameters are identified: the flame filter size, the sub-filter flame wrinkling and the number of flame patterns contained within the sub-filter volume. This new flame archetype, named Filtered Wrinkled Flamelets (FWF), may be embedded in various combustion modeling frameworks. In the present paper, it is used to build-up a filtered chemical look-up table in order to model the unclosed terms of the filtered progress variable equation. *A priori* tests are conducted by analyzing an existing turbulent premixed flame database. *A posteriori* tests consist in modeling the swirling bluff-body stabilized Cambridge flame. Results analysis shows that accounting for sub-filter flame wrinkling on the chemical flame structure is mandatory to predict intermediate species such as CO.

1. Introduction

Introduction of detailed chemistry effects in numerical simulation of turbulent flames is an ultimate objective for the combustion modeling community [1]. Despite the great challenge to overcome, this effort is mandatory to predict complex phenomena such as flame ignition or extinction and also pollutant formation. Several methods have been conducted to account for detailed chemistry in a Large-Eddy Simulation context [2] for a CPU cost, which remains reasonable, so that the simulation of practical industrial reactive systems is possible. Among them, geometrical formulations have been designed to capture the flame front propagation and thus to represent accurately the flame dynamics in premixed or stratified combustion regimes in LES [3].

Examples of existing approaches based on a geometrical formulation are the G-equation [4–7], filtered one-dimensional flames [8–11] and thickened flame model [12–14]. These approaches are designed to capture accurately the turbulent flame consumption speed in the flamelet regime whether or not the flame thickness and wrinkling are resolved at the LES sub-filter scale. The sub-filter scale flame wrinkling Ξ_Δ, generally modeled either by algebraic [15–17] or dynamical [18–20] procedures, is coupled to the reactive flow equations so that both the source and turbulent diffusion terms of chemical species balance equations (or progress variable) are enhanced by a factor Ξ_Δ. Consequently, the turbulent flame front propagates at a speed $S_\Delta = \Xi_\Delta S_L^0$, where S_L^0 is the unstrained laminar flame consumption speed. A recent comparative study, conducted on a turbulent stratified flame configuration experimented at T.U. Darmstadt [21], indeed confirms that geometrical-based numerical approaches perform well when focusing on the turbulent flame front position [22].

The impact of the sub-filter scale flame wrinkling on the filtered flame chemical structure has however never been considered. Indeed, geometrical approaches for flamelet regime usually assume that the filtered flame thickness and chemical profiles are not affected by sub-filter scale flame wrinkling. This assumption has been questioned by Moureau et al. [11] who observed, through the analysis of the DNS of a turbulent premixed swirled flame, that filtered quantities are also influenced by the surface of the flame contained at the sub-filter scale. Several families of modeling approaches implicitly account for the impact of sub-filter state on the resolved quantities such as *(i)* Linear-Eddy

* Corresponding author.
E-mail address: renaud-c.mercier@safrangroup.com (R. Mercier).

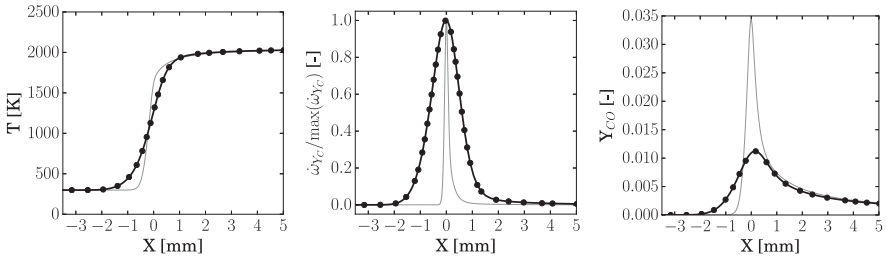

(a) Temperature (b) Normalized progress variable reaction rate $\dot{\omega}_{Y_C}/\max(\dot{\omega}_{Y_C})$ (c) CO mass fraction

Fig. 1. Differences between thickened and filtered flame structures. Both filtered and thickened flames have identical thermal layer thicknesses. Legend : — Laminar detailed chemistry solution, — Detailed chemistry solution, filtered at a size $\Delta = 2$ mm, ••• F-TACLES solution..

model [23] where empirical mean of perturbed states are used; *(ii)* PDF-based models were the sub-filter state is described through a presumed [24] or transported PDF [25]. These approaches are however difficult to express in a geometrical formalism.

The objective of the present article is to model the impact of the sub-filter scale flame wrinkling on the chemical flame structure and therefore on the minor species production and destruction, which is important for predicting pollutant emissions. A focus here is made on the carbon monoxide (CO) species. The unclosed terms of the progress variable equation are modeled following an approach similar to the Filtered Tabulated Chemistry for LES (F-TACLES) model [10], where a chemical look-up table is generated from Filtered Planar Flamelet (FPF) elements that are computed *a priori* using a 1-D flame solver including detailed chemistry and complex transport. The major issue of this approach is to incorporate the flame wrinkling in the look-up table generation. For that purpose, the standard planar flamelet assumption of F-TACLES is revisited by manufacturing a series of 2-D wrinkled flames with analytical wrinkling patterns. The paper is organized as follows. Section 2 presents the *a priori* study of the impact of sub-filter scale flame wrinkling on the filtered chemical flame structure. Section 3 describes the procedure to generate a series of 2-D wrinkled flames with analytical wrinkling patterns. The explicit filtering of these manufactured solutions serves to compute a database that relates filtered thermochemical quantities to the flame wrinkling patterns. A turbulent combustion model using the Filtered Wrinkled Flamelets (FWF) is derived in Section 5. Its *a priori* validation against a filtered DNS database is then conducted in Section 6. Finally, LES of the Cambridge premixed flame burner [26] is computed and compared to experimental data in Section 7.

2. *A priori* study of the impact of sub-filter scale flame wrinkling on the filtered chemical flame structure

Two scales are often unresolved in Large Eddy Simulation of turbulent premixed or stratified flames: the flame thickness and the small-scale flame wrinkling.

The first one, the laminar flame thickness, is in general smaller than the grid size in most practical meshes [3]. To avoid the under-resolution of the reactive layer and therefore a mis-prediction of the flame propagation speed, Thickened Flame model for LES (TFLES) artificially thickens the flame front by a factor F [12]. TFLES does not reproduce however some specific sub-grid scale phenomena for intermediate species. An alternative to thickened flame model are Filtered Planar Flamelet (FPF) based models such as F-TACLES [10], where reference flamelets are filtered, tabulated and stored in a look-up table.

Filtered Planar Flamelet approach is illustrated in Fig. 1 by post-processing the detailed chemistry solution of a laminar freely-propagating 1-D methane-air flame computed with the REGATH solver [27] using the mechanism proposed by Lindstedt [28] at an equivalence ratio $\phi = 0.83$ and atmospheric pressure. The reactive flame thickness, defined here as the full width at half maximum (FWHM) of the heat release, is $\delta_r = 0.17$ mm. The thermal flame thickness, defined from unburnt gas temperature T^u and burnt gas temperature T^b as $\delta_l^0 = (T^b - T^u)/\max(\nabla T)$, is $\delta_l^0 = 0.53$ mm. To mimic a reference *ideal* laminar LES flame solution, the detailed chemistry temperature and CO mass fraction profiles are filtered by a Gaussian function of width Δ. Profiles of temperature T, normalized progress variable reaction rate $\dot{\omega}_{Y_C}/\max(\dot{\omega}_{Y_C})$ and CO mass fraction Y_{CO} are plotted in Fig. 1 for $\Delta = 2$ mm.

The effective ratio $\Delta/\delta_r = 11.2$ is well representative of practical reactive LES configurations, where the flame thickness is smaller than the filter associated to the flame [29]. An advantage of the filtering formalism is the conservation of the mass of chemical species contained within the flame layer as discussed in [10]. Figure 1 presents an *a priori* reconstruction of the filtered temperature and CO mass fractions extracted from a FPF look-up table. For a 1-D unstrained laminar flame (*i.e.* without any sub-filter wrinkling) F-TACLES recovers the filtered laminar flame structure as expected.

The second unresolved scales are flame wrinkling patterns smaller than the filter size. The impact of sub-filter scale flame wrinkling Ξ_Δ on the filtered flame propagation speed is well accounted for in F-TACLES models [10]. However this formulation assumes that the filtered chemical flame structure is not altered by sub-filter scale eddies (*i.e.* the flame is planar at the sub-filter scale). This assumption is challenged by the post-processing of turbulent premixed flame DNS data obtained by Moureau et al. [11] of the PRECCINSTA combustion chamber [30]. The configuration, which features a plenum, a swirl-injector and a combustion chamber, is representative of aeronautical combustion devices. DNS flame data are filtered at a size $\Delta = 11.2\delta_r$. The Favre-filtered temperature and CO mass fraction fields are then conditionally-averaged on iso-contours at a given distance to the filtered flame front position. This filtered flame front position is defined as the iso-contour $\tilde{c} = 0.8$, where $\tilde{c}$ is the Favre-filtered normalized progress variable. The conditional averages are plotted in Fig. 2. Diamond and plus symbol lines show *references* profiles obtained at two axial distances to the burner head, $z = 1$ cm and $z = 4$ cm, respectively. While the first axial position is located at the anchoring of the flame, the second position is at its tip. The wrinkling of the flame increases further downstream in the combustor, and the two axial positions correspond to two different sub-filter scale flame wrinkling conditions: $\Xi_\Delta = 1.2$ at $z = 1$ cm,

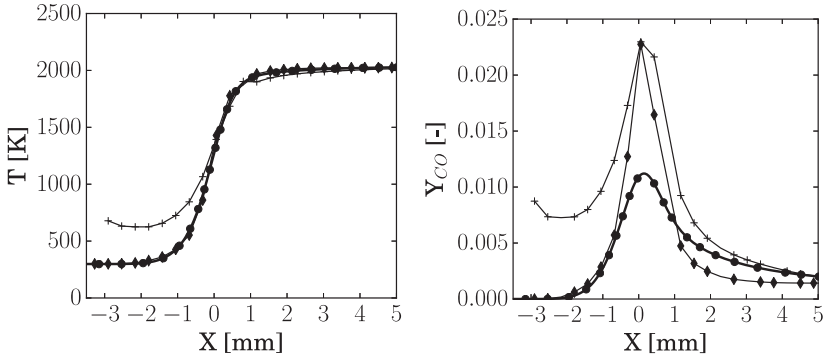

Fig. 2. Filtered temperature and CO mass fraction profiles obtained by post-processing a DNS solution of the PRECCINSTA configuration. Legend : ♦—♦ Filtered DNS solution ($\Xi_\Delta = 1.2$), +–+ Filtered DNS solution ($\Xi_\Delta = 2.0$), ●—● F-TACLES solution.

whereas $\Xi_\Delta = 2$ at $z = 4$ cm. It can be noted that for the second position, where the flame is highly corrugated, multiple front-front interactions occur, which leads to an increase of the temperature and the CO mass fraction on the fresh gas side for $X < -2$ mm. The filtered chemical flame structure *a priori* predicted by F-TACLES is reconstructed by post-processing the DNS progress variable field with a filtered look-up table built from Planar Flamelets filtered at $\Delta = 11.2\delta_r$ (FPF) as in the post-processed DNS. As discussed in [11], the sub-filter scale flame wrinkling tends to increase the filtered flame thickness. It leads to a slight underestimation of the thermal layer by F-TACLES as observed in Fig. 2, which is emphasized when Ξ_Δ increases. The discrepancies are considerably more significant for the CO mass fraction. Indeed, neglecting the impact of sub-filter scale flame wrinkling on the carbon monoxide production causes an 50% underestimation of CO peak in this case.

While the impact of sub-filter scale flame wrinkling on the flame thermal layer remains marginal, its effect on intermediate species prediction is pronounced. In the following section, a methodology named Filtered Wrinkled Flamelets (FWF) is proposed to include sub-filter scale wrinkling in the filtered flamelets formalism.

3. Modeling the impact of the sub-filter scale wrinkling on the filtered flame properties

The influence of sub-filter scale wrinkling on the chemical flame structure is in practice difficult to anticipate and describe analytically. In this section, manufactured flame solutions are used to study the relation between the filtered flame properties (such as consumption speed, thickness, and species profiles) with the geometrical properties of the wrinkled flame at the sub-filter scale.

3.1. Problem model

The impact of the geometrical properties of a 2-D wrinkled flame on the filtered flame structure is analyzed. Assuming that the sub-filter flame is in the flamelet regime, the flame front is tracked by a progress variable c equal to 0 and 1 in fresh and burnt gases, respectively. A 2-D wrinkled flame pattern, shown in Fig. 3, is manufactured by assuming that the coordinates $(x_{c=c_0}, y_{c=c_0})$ of the iso-line $c = c_0$ are related by a sinusoidal function: $x_{c=c_0} = A\sin(2\pi y_{c=c_0}/L_y)$, with A the amplitude of the sinusoidal iso-line and L_y its wavelength. This flame pattern is embedded in a 2-D square of size Δ, the flame filter size, to mimic a sub-filter scale domain. For simplicity, the flame is not wrinkled in the spanwise direction. The model could be easily extended with 3-D manufactured solutions. A 2-D approach is however preferred here as it simplifies the model formalism as well as its analysis in a first approach.

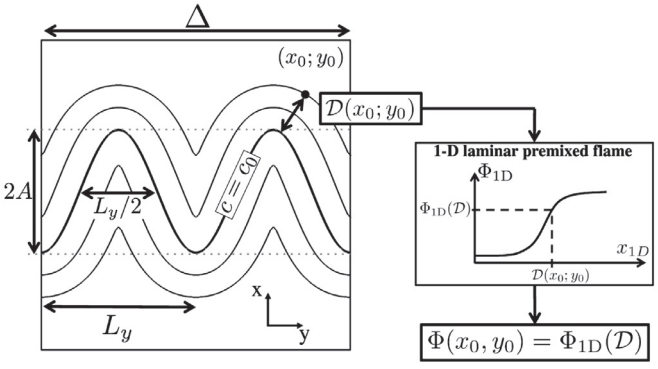

Fig. 3. Schematic view of sub-filter sinusoidal flame pattern with $n_\Delta = \Delta/L_y = 2$. The mapping process of a thermochemical quantity Φ onto a 1-D premixed laminar flame computed with detailed chemistry is also presented.

The number of wavelengths contained within the box is given by $n_\Delta = \Delta/L_y$. As discussed in the BML analysis [31], $2n_\Delta$ corresponds to the average number of flame crossings of a specified line per unit distance Δ. We suppose here that n_Δ is an integer. For a given flame filter size Δ, the sub-filter flame pattern is then periodic and parametrized by two parameters: n_Δ controls the wavelength while A controls the amplitude of the $c = c_0$ iso-line. The sub-filter scale wrinkling is determined by the pair (A, n_Δ). For $n_\Delta = 0$ or $A = 0$ the flame remains planar while for $A > 0$, the flame is wrinkled as soon as $n_\Delta \geq 1$. The possible range of variation of both A and n_Δ is discussed in the following.

3.2. Physical range of variation of model parameters A and n_Δ

Assuming a flamelet regime, the size of the smallest eddy having a turnover velocity sufficient to wrinkle the flame front is the Gibson length L_G [32]:

$$L_G = \frac{(S_l^0)^3}{\epsilon} = \left(\frac{S_l^0}{u'_\Delta}\right)^3 \Delta \tag{1}$$

where S_l^0 is the laminar flame speed, u'_Δ quantifies the sub-filter velocity fluctuations and ϵ is the kinetic energy transfer rate, assumed here within the inertial range. The flame wrinkling length scale $L_y/2$, illustrated in Fig. 3, should therefore be larger than L_G. As discussed by [3,32] in the flamelet regime (*i.e.* thin flame regime), L_G varies between the integral length scale L_t and the size of the smallest eddy η which is larger than the flame thickness δ_l^0. The minimal value of the flame front wavelength reads:

$$L_y^{min} = 2L_G > 2\delta_l^0 \tag{2}$$

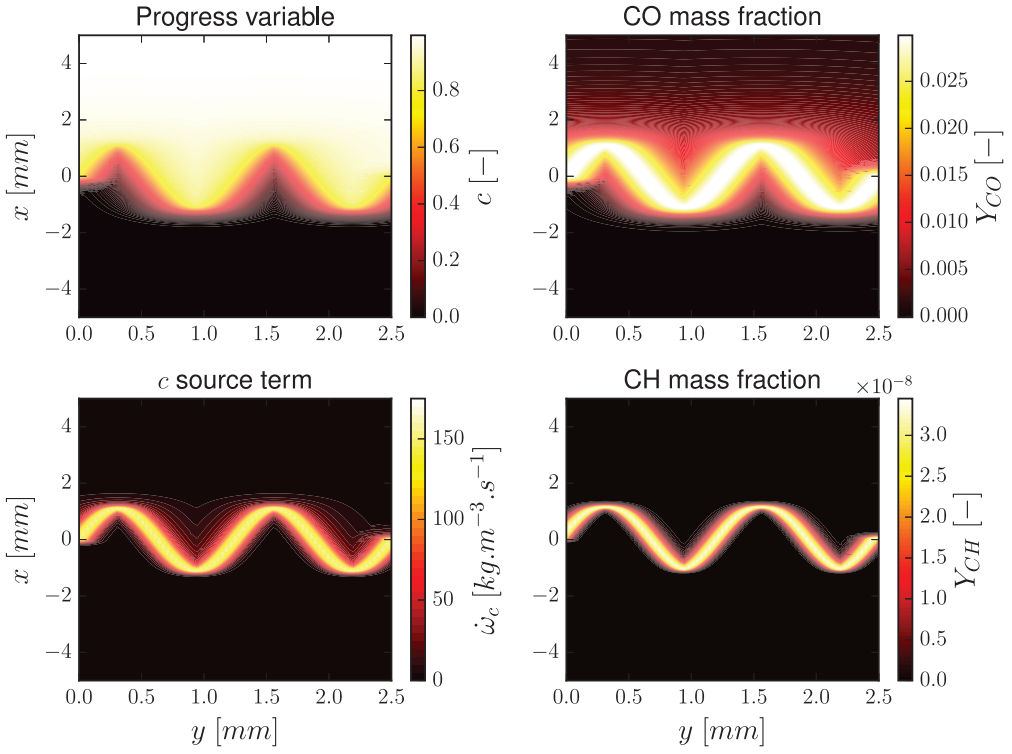

Fig. 4. Representation of 2-D manufactured thermochemical variables for $\Delta/\delta_l^0 = 5$, $\Xi_\Delta = 3$ and $n_\Delta = 2$. Top left: progress variable c. Top right: CO mass fraction Y_{CO}. Bottom left: progress variable reaction rate $\dot{\omega}_c$. Bottom right: CH radical mass fraction Y_{CH}.

As n_Δ is assumed to be an integer, the maximal number of flame wrinkling patterns n_Δ^{max} is therefore given by:

$$n_\Delta^{max} = \mathrm{E}\left[\frac{\Delta}{L_y^{min}}\right] \tag{3}$$

where $E[r]$ is the integer part of r.

In the flamelet regime, the local flame front curvature κ has also to remain smaller that a threshold value so that the flame structure is unaltered. Thus, the radius of curvature $R = 1/\kappa$ has to be larger than the cut-off length scale δ which is of the order of the laminar flame thickness [3]. As the flame front geometry is modeled by a sinusoidal pattern of normal $\mathbf{n}$, the analytical expression for $\kappa = \nabla \cdot \mathbf{n}$ reads:

$$\kappa = A\left(\frac{2\pi}{L_y}\right)^2 \frac{|\sin(2\pi y_{c=c_0}/L_y)|}{[1 + A^2(2\pi/L_y)^2\cos^2(2\pi y_{c=c_0}/L_y)]^{3/2}} \tag{4}$$

The maximal value of κ observed along the sinusoidal flame front is observed for $y_{c=c_0} = L_y/4$:

$$\max \kappa\,(y_{c=c_0}) = A\left(\frac{2\pi}{L_y}\right)^2 \tag{5}$$

The flamelet condition $R > \delta$ combined with Eq. (5) gives the maximum possible amplitude A^{max} of the sinusoidal pattern:

$$A^{max} = \frac{L_y^2}{4\pi^2\delta} \tag{6}$$

Equations (3) and (6) give the maximal physical value of both A and n_Δ parameters so that the wrinkled flame pattern remains within the flamelet regime. Based on this assumption, the wrinkled flame structure is reconstructed from a 1-D flamelet in the following section.

3.3. Estimating filtered quantities from a presumed sub-filter flame pattern

Assuming that the flame is in the flamelet regime, the 2-D flame structure is manufactured from a 1-D laminar premixed flame computed with detailed chemistry. The shortest distance $\mathcal{D}(x, y)$ between each point (x, y) contained in the 2-D sub-filter domain and the iso-line $c = c_0$ is introduced as illustrated in Fig. 3. The thin reaction zone position $c = c_0$ is located at the maximal heat release point of the flame. The $\mathcal{D}$ field is then used to map any thermochemical quantity Φ using the 1-D flamelet data:

$$\Phi(x, y) = \Phi_{1D}(\mathcal{D}(x, y))\,, \tag{7}$$

where Φ_{1D} denotes the 1-D flamelet thermochemical quantities. An example of 2-D manufactured fields is given in Fig. 4 for the progress variable c, its source term $\dot{\omega}_c$, CO mass fraction Y_{CO} and CH mass fraction Y_{CH}.

Filtered quantities $\overline{\Phi}$ are defined by:

$$\overline{\Phi}(x, y) = \int_{-\infty}^{+\infty}\int_{-\infty}^{+\infty} \Phi(x', y') F_\Delta^{2D}(x - x', y - y')\,dx'dy'\,, \tag{8}$$

where F_Δ^{2D} is a 2-D box filter of size Δ. By introducing F_Δ^{1D}, the 1-D box filter of size Δ, $F_\Delta^{2D}(x, y)$ is decomposed as $F_\Delta^{1D}(x)F_\Delta^{1D}(y)$ and $\overline{\Phi}$ also reads:

$$\overline{\Phi}(x, y) = \int_{-\infty}^{+\infty} F_\Delta^{1D}(x - x')\left[\int_{-\infty}^{+\infty} \Phi(x', y') F_\Delta^{1D}(y - y')dy'\right]dx'\,. \tag{9}$$

As the flame pattern is $n_\Delta L_y$-periodic at the sub-filter scale in the y-direction, the filtering along y reduces to an averaging operation over a single wavelength:

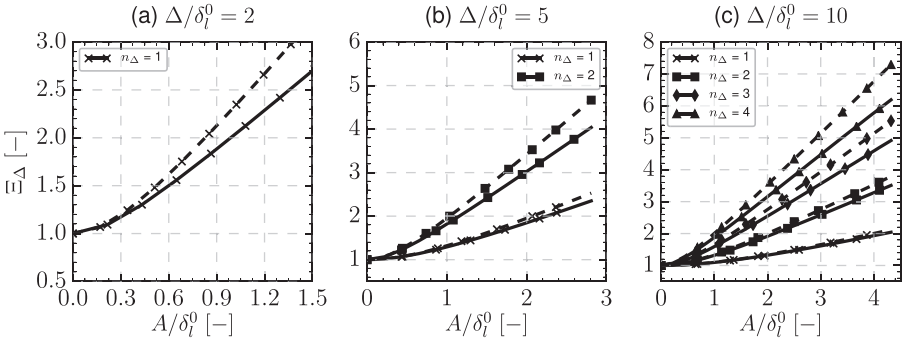

Fig. 5. Sub-filter scale wrinkling Ξ_Δ as a function of the normalized amplitude A/δ_l^0 for different n_Δ and normalized filter sizes Δ/δ_l^0. Legend: — Manufactured wrinkled flamelet integration (Eq. (12)); – – Infinitely thin flame assumption (Eq. (13)).

$$\overline{\Phi}(x) = \int_{-\infty}^{+\infty} F_\Delta^{1D}(x-x') \underbrace{\frac{1}{L_y}\left[\int_{-L_y/2}^{+L_y/2} \Phi(x',y')dy'\right]}_{\overline{\Phi}^y(x')} dx' . \tag{10}$$

Therefore, any filtered quantity associated to the periodic wrinkled flame pattern varies only along x coordinate and reads:

$$\overline{\Phi}(x) = \int_{-\infty}^{+\infty} F_\Delta^{1D}(x-x')\overline{\Phi}^y(x')dx' . \tag{11}$$

3.4. Link between sub-filter scale pattern and wrinkling

The sub-filter flame wrinkling is defined as:

$$\Xi_\Delta = \frac{S_\Delta}{S_l^0} = \frac{1}{\rho_0 S_l^0}\int_{-\infty}^{+\infty} \overline{\dot{\omega}}_c(x)dx , \tag{12}$$

where the filtered progress variable reaction rate $\overline{\dot{\omega}}_c$ is computed from Eq. (11). For a given LES filter size Δ, the presumed flame pattern and its wrinkling Ξ_Δ are parametrized by both $n_\Delta = \Delta/L_y$ and the amplitude A. An analytical relation between Ξ_Δ and $\xi = n_\Delta A/\Delta$ is obtained under infinitely thin flame assumption ($\Delta/\delta_l^0 \to \infty$):

$$\Xi_\Delta = \frac{\sqrt{(2\pi\xi)^2+1}}{2\pi}\mathrm{EI}\left(2\pi, 1-\frac{1}{(2\pi\xi)^2+1}\right), \tag{13}$$

where EI is the incomplete elliptic integral of the second kind. However, in the general case where the flame thickness is considered, a numerical integration is needed to compute Eq. (12).

4. Analysis of Filtered Wrinkled Flamelet consistency

To illustrate the methodology, 2-D wrinkled flames are manufactured for a given pair (A, n_Δ) using Φ^{1D} variables from a 1-D CH_4-air flame computed at $\phi = 0.83$ using detailed chemistry [28]. The progress variable is defined as $c = Y_c/Y_c^{eq}$, where $Y_c = Y_{CO} + Y_{CO_2} + Y_{H_2O}$ and eq superscript denotes equilibrium conditions. Manufactured 2-D variables Φ are then numerically filtered according to Eq. (11) for a given filter width Δ.

4.1. Evolution of Ξ_Δ with A

Figure 5 shows Ξ_Δ as a function of A/δ_l^0 for different values of n_Δ and Δ/δ_l^0. Solid lines are obtained from the numerical integration of Eq. (12), whereas dashed lines represent the analytical solutions given by Eq. (13) under infinitely thin flame assumption. For a planar flame ($A = 0$), the flame wrinkling Ξ_Δ equals 1. When A increases, Ξ_Δ increases as expected. The dependency of Ξ_Δ to the pair (A, n_Δ) is clearly evidenced in Fig. 5 as, for a given amplitude A and filter size Δ, Ξ_Δ increases with the number of wavelengths n_Δ. The analytical model given by Eq. (13) is retrieved as long as A and n_Δ remain small, which is in line with the bounds proposed in Eq. (6). Flame thermal and reactive layers are indeed overlapping at the sine wave peaks when A reaches the critical value $A^{\max}$ and the numerically computed wrinkling ratio thus decreases compare to infinitely thin flame case. It is important to note that the model degenerates towards DNS when $\Delta \to 0$: as the filter size vanishes the bound imposed on n_Δ due to the flame cut-off implies that no analytical wrinkling is possible and hence the flame stays planar.

Figure 5 also shows that, for a given Δ and n_Δ, there is a unique correspondence between A and Ξ_Δ. Filtered variables can therefore be parametrized by $(\Xi_\Delta, n_\Delta, \Delta)$ instead of (A, n_Δ, Δ). This formulation is preferred for practical reasons: many accurate LES model for the subgrid scale flame wrinkling exists in the literature (unlike to the subgrid flame wrinkling amplitude)

4.2. Effect of wrinkling on flame thickness

Filtered data are also post-processed to compute, for the set of parameters $(\Xi_\Delta, n_\Delta, \Delta)$, the filtered flame thickness $\delta_{\tilde{c}} = 1/\max(|\nabla\tilde{c}|)$. $\delta_{\tilde{c}}$ is plotted in Fig. 6 as a function of Ξ_Δ for different values of n_Δ. A strong dependency of the flame thickness $\delta_{\tilde{c}}$ to Ξ_Δ is observed for any of the three filter sizes considered. When $\Delta/\delta_l^0 > 2$, the number of wavelengths n_Δ influences significantly the filtered flame thickness. Indeed, for a given Ξ_Δ, $\delta_{\tilde{c}}$ decreases when n_Δ increases. In this last case, $\delta_{\tilde{c}}$ tends to the filter size Δ because, for a given Ξ_Δ, the amplitude of the flame pattern A gets smaller compared to Δ. For small values of n_Δ, A needs to be larger to reach a given level of wrinkling (see Fig. 5) which leads to an increasing filtered flame thickness $\delta_{\tilde{c}}$. This behavior is also illustrated by Fig. 7 which shows filtered progress variable $\tilde{c}$ and filtered chemical reaction rate $\overline{\dot{\omega}}_c$ for different values of Δ/δ_l^0, n_Δ and Ξ_Δ. For a given n_Δ, the flame thickness increases due to wrinkling (left plot). Larger wrinkling values also modify the filtered reaction rates profiles (right plot) to larger maximum values. For a given wrinkling value Ξ_Δ, the flame thickness decreases when n_Δ increases since the sine amplitude A reduces for constant Ξ_Δ.

This analysis shows that for a given filter size Δ, the filtered flame structure depends on both Ξ_Δ and n_Δ. It means that Ξ_Δ is *a priori* not sufficient to determine the filtered flame structure, which is also influenced by the geometrical shape of the flame at the sub-filter scale.

4.3. Effect of wrinkling on sub-filter species mass

Figure 8 shows the evolution of the mass of CO m_{CO} contained in a sub-filter box of size Δ as a function of the wrinkling Ξ_Δ of the flame pattern. To ease the interpretation, $m_{CO}(\Xi_\Delta)$ is normalized by the mass of CO of the planar flame $m_{CO}(\Xi_\Delta = 1)$. For

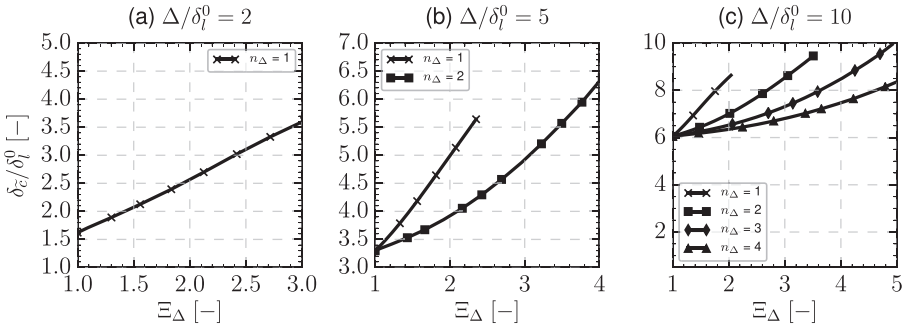

Fig. 6. Comparison of the ratio $\delta_{\tilde{c}}/\delta_l^0$ as a function of the sub-filter scale wrinkling Ξ_Δ for different values of n_Δ and different normalized filter sizes Δ/δ_l^0.

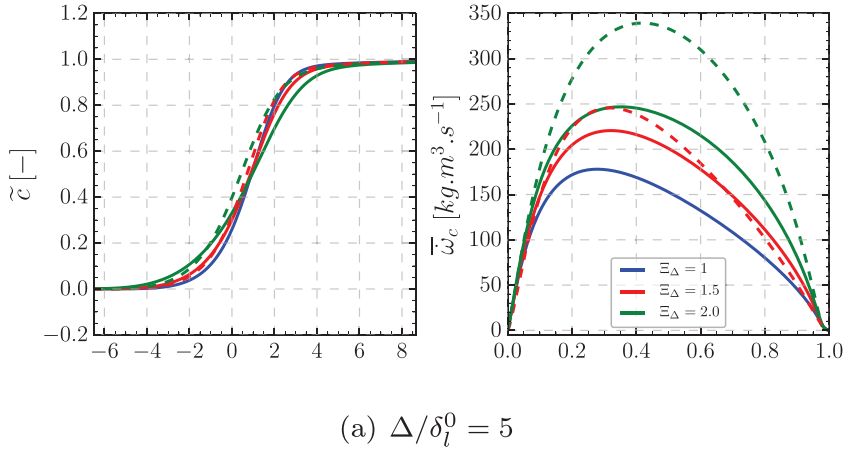

(a) $\Delta/\delta_l^0 = 5$

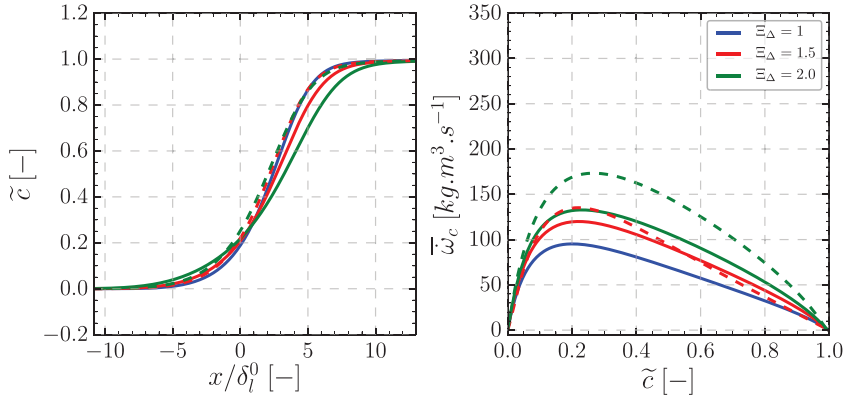

(b) $\Delta/\delta_l^0 = 10$

Fig. 7. Favre-filtered progress variable $\widetilde{c}$ as a function of dimensionless position x/δ_l^0 (left) and filtered reaction rate $\overline{\dot{\omega}}_c$ as a function of $\widetilde{c}$ (right) for different values of wrinkling ratio Ξ_Δ and filter width Δ/δ_l^0. Legend: Solid lines: FWF $n_\Delta = 1$; Dashed lines: FWF $n_\Delta = 2$.

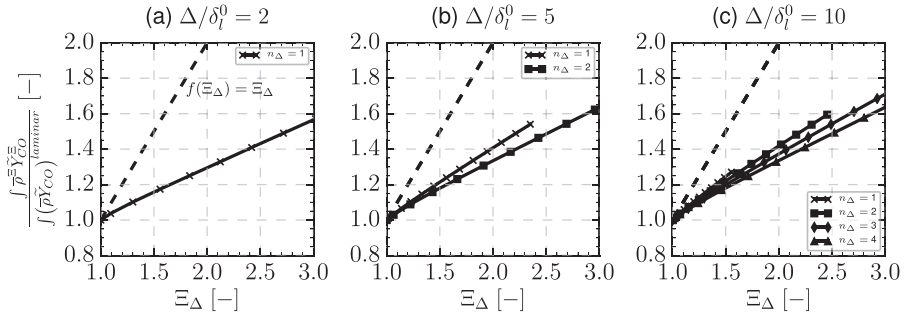

Fig. 8. Normalized mass of CO in the sub-filter box as a function of the wrinkling ratio Ξ_Δ for different values of Δ/δ_l^0 and n_Δ. Dashed line shows unitary line $f(\Xi_\Delta) = \Xi_\Delta$.

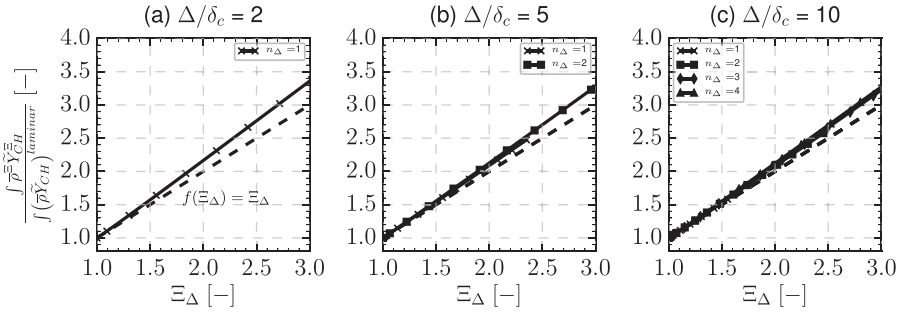

Fig. 9. Normalized mass of CH in the sub-filter box as a function of the wrinkling ratio Ξ_Δ for different values of Δ/δ_l^0 and n_Δ. Dashed line shows unitary line $f(\Xi_\Delta) = \Xi_\Delta$.

a given flame pattern of wrinkling Ξ_Δ, $m_{CO}(\Xi_\Delta)$ is computed by integrating ρY_{CO} over the surface:

$$m_{CO}(\Xi_\Delta) = \int_{x=-\Delta/2}^{\Delta/2} \int_{y=0}^{\Delta} \rho(x,y) Y_{CO}(x,y) \mathrm{d}y\mathrm{d}x \tag{14}$$

Several curves are presented for different values of Δ/δ_l^0 and n_Δ. As expected, the main observation is that m_{CO} increases with Ξ_Δ due to the increased flame surface within the box. m_{CO} is relatively independent from the value of n_Δ and is however much lower than the unitary line $m_{CO}(\Xi_\Delta) = \Xi_\Delta m_{CO}(\Xi_\Delta = 1)$ which corresponds to the theoretical value of the integral that would be obtained if the CO mass was concentrated on the sine pattern (*i.e.* for an infinitely thin front). This departure of m_{CO} is mainly due to the non-zero Y_{CO} value in the burnt gases which implies that some fraction of CO mass is located outside of the filter volume when the manufactured wrinkled flame is constructed. This is verified by carrying out the same analysis for CH radical which has a much lower thickness (as seen in Fig. 4) and a zero value in both fresh and burnt gases. The resulting CH mass m_{CH} shown in Fig. 9 is accurately approximated by the unitary line. The remaining gap increases with Ξ_Δ and is due to profile thickness effects in high curvature regions. In this case only, the following approximation therefore applies:

$$m_{CH}(\Xi_\Delta) \approx \Xi_\Delta m_{CH}(\Xi_\Delta = 1) \tag{15}$$

In the more general case of thicker species profiles compared to Δ or to a species with non-zero mass fractions in fresh or burnt gases, the filtered species mass fractions cannot be approximated by simple relations such as Eq. (15).

4.4. Comparison of Filtered Wrinkled Flame structure against DNS data

The approximations made to manufacture the Filtered Wrinkled Flamelets neglect several physical phenomena such as curvature or stretch effects. In order to estimate the impact of these assumptions, the FWF database is compared against DNS solution [11,30] of a turbulent premixed flame previously introduced in Section 2. To enable a direct comparison between DNS and the FWF database, the filtered flame thickness is now defined as:

$$\delta_{\tilde{c}}^0 = 1/|\nabla \tilde{c}|_{\tilde{c}=\tilde{c}_0} \tag{16}$$

where $\tilde{c}_0$ is a progress variable iso-line value chosen to be close to the region of maximal $|\nabla\tilde{c}|$. The sub-grid scale flame wrinkling is computed in the DNS as $\Xi_\Delta = \overline{|\nabla c|}/|\nabla \overline{c}|$. For a given filter size, both the filtered flame thickness and the sub-grid scale flame wrinkling are then estimated in the DNS solutions along the flame surface defined as $\tilde{c}_0$ iso-line. The filtered flame thickness conditioned by the sub-grid scale flame wrinkling is shown in Fig. 10 for three values of filter sizes: $\Delta/\delta_l^0 = 2$, 5 and 10. The filtered flame thickness defined at $\tilde{c}_0 = 0.5$ is computed from the reference DNS data (solid plain line) and the approximate Filtered Wrinkled Flamelet database (solid line with symbols) for different values of n_Δ. The gray area represents the variability of $\delta_{\tilde{c}}^0/\delta_l^0$ for a given wrinkling value Ξ_Δ: the upper and lower thin lines correspond to plus and minus the RMS, respectively. As the filtered flame thickness is strongly dependent on the flame wrinkling in the DNS and on the n_Δ parameter in the FWF model, this figure gives an indication on the n_Δ parameter that should be used in the FWF model to recover the DNS filtered flame thickness. The n_Δ value that should be chosen depends on the non-dimensional filter size Δ/δ_l^0: n_Δ should increase with the filter size. Moreover, a single value per filter size would already give an acceptable model since $1 \leq n_\Delta \leq 2$ for $\Delta/\delta_l^0 \leq 10$ for the DNS considered here.

The prediction of CO filtered reaction rate given by the FWF database is also assessed by comparison with the DNS database. For that purpose, Fig. 11 illustrates the impact of both n_Δ and Ξ_Δ on the filtered CO mass fraction profile $\widetilde{Y}_{CO}$ for a given filter width Δ/δ_l^0 (left plot). $\widetilde{Y}_{CO}$ profile thickness and peak value are clearly impacted by both parameters. The solid blue curve ($\Xi_\Delta = 1$) also corresponds to the original F-TACLES. Significant differences with the $\Xi_\Delta = 1.5$ and $\Xi_\Delta = 2$ curves illustrates the gain of the model improvement. CO filtered reaction rate $\overline{\dot{\omega}}_{CO}$ extracted from FWF database is then compared to the post-processed DNS for both $\Delta/\delta_l^0 = 5$ and 10 (right plot). DNS mean and RMS values of $\overline{\dot{\omega}}_{CO}$ conditioned to $\widetilde{c}$ are shown by black line and gray filled area, respectively. The trends of the DNS mean profiles are well reproduced by the FWF database. The FWF profiles variations due to n_Δ and Ξ_Δ are also in line with the RMS values of the post-processed DNS. The slight differences observed are certainly due to modeling hypothesis, which include the sinusoidal shape of the flame surface and the canonical unstrained 1-D laminar flame profile used to manufacture the wrinkled flamelets. It confirms that the Filtered Wrinkled Flames archetypes are able to tackle the impacts of actual sub-filter scale wrinkling patterns on the resolved intermediate species profiles through n_Δ and Ξ_Δ parameters.

5. Closure of the filtered progress variable balance equation using Filtered Wrinkled Flamelets (FWF)

5.1. Filtered Wrinkled Flamelet database

A series of filtered wrinkled flamelets is manufactured by varying A and Δ for a given wavelength parameter n_Δ. For each set of geometrical parameters, filtered thermochemical variables $\overline{\Phi}$ are mapped in the filtered progress variable $\tilde{c}$ space as in [10]. As discussed in Section 4.1, a set of parameters (A, Δ) corresponds, for a given n_Δ, to a unique value of Ξ_Δ. Therefore $\overline{\Phi}$ can be mapped and tabulated as:

$$\overline{\Phi} = \overline{\Phi}[\widetilde{c}, \Delta, \Xi_\Delta]_{n_\Delta}. \tag{17}$$

An illustration of the FWF table is shown in Fig. 7 for a CH_4-Air premixed flame at $\phi = 0.83$ filtered at $\Delta = 5\delta_l^0$ (top right)

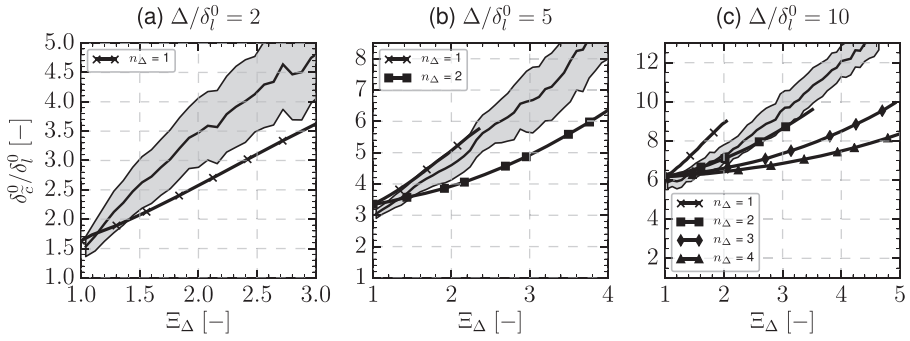

Fig. 10. Comparison of δ_c^0/δ_l^0 computed for $\tilde{c}_0 = 0.5$ as a function of the sub-filter scale wrinkling Ξ_Δ for different values of n_Δ and different normalized filter sizes Δ/δ_l^0. Legend: Solid lines with symbols: FWF database. Solid line: DNS Mean value. Filled area: plus and minus the standard deviation.

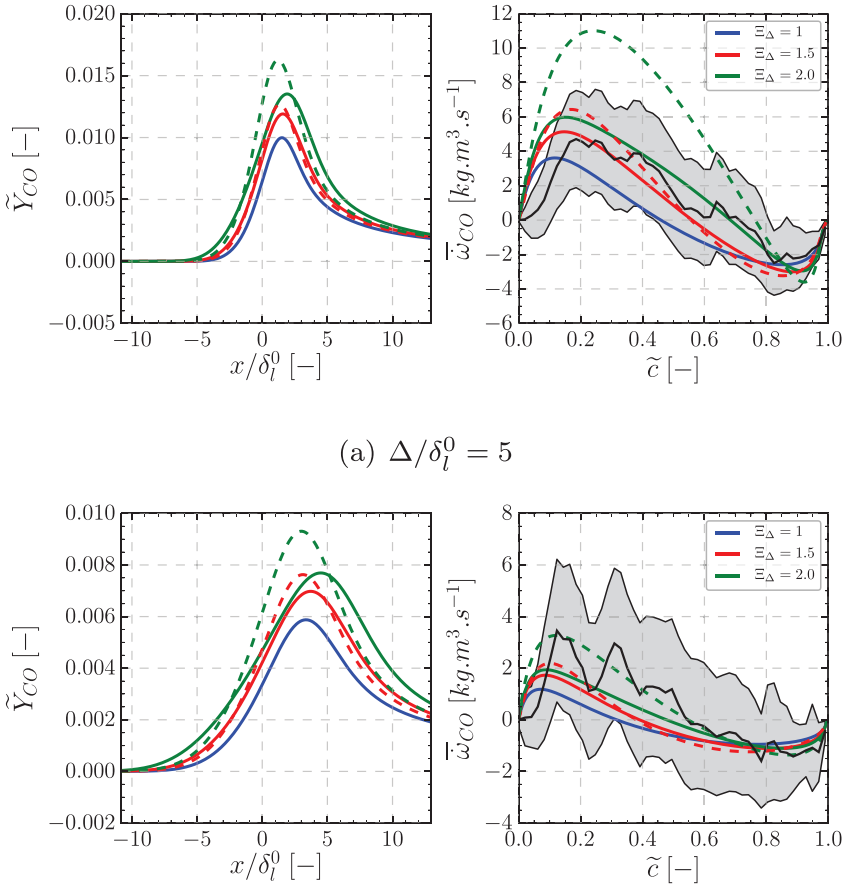

Fig. 11. Favre-filtered CO mass fraction $\widetilde{Y}_{CO}$ as a function of dimensionless position x/δ_l^0 (left) and filtered chemical reaction rate $\overline{\dot{\omega}}_{CO}$ as a function of the filtered progress variable $\tilde{c}$ (right) for different values of wrinkling ratio Ξ_Δ and filter width Δ/δ_l^0. Legend: Solid colored lines: FWF $n_\Delta = 1$; Dashed colored lines: FWF $n_\Delta = 2$; Solid black line: DNS Mean value. Filled area: plus and minus the standard deviation.

and $\Delta = 10\delta_l^0$ (bottom right). The evolution along the $\tilde{c}$ coordinate of the filtered progress variable reaction rate $\overline{\dot{\omega}}_c$ is shown for different values of Ξ_Δ and n_Δ. In both figures, the profiles of $\overline{\dot{\omega}}_c$ for $\Xi_\Delta = 1$ match as expected regardless of the value of n_Δ. They also correspond to the filtered laminar reaction rate that would be extracted from the 1-D filtered premixed flame. It corresponds to the case where the flame is planar at the sub-filter scale. However, when $\Xi_\Delta = 1.4$ and $\Xi_\Delta = 2.5$, $\widetilde{\dot{\omega}}_c$ differs depending on n_Δ as discussed in Section 3.4. This effect is exacerbated as Ξ_Δ increases.

5.2. Closure of the filtered progress variable equation

In LES, the filtered progress variable $\tilde{c}$ is governed by the following equation:

$$\frac{\partial \overline{\rho}\tilde{c}}{\partial t} + \nabla \cdot \overline{\rho}\tilde{\mathbf{u}}\tilde{c} = \nabla \cdot (-\overline{\rho \mathbf{V_c}}) + \nabla \cdot \overline{\rho}(\tilde{c}\tilde{\mathbf{u}} - \widetilde{c\mathbf{u}}) + \overline{\dot{\omega}}_c\,, \tag{18}$$

where $\overline{\rho}$ is the filtered density, $\tilde{\mathbf{u}}$ is the filtered velocity, $\mathbf{V_c}$ is the molecular diffusion velocity of the progress variable and $\overline{\dot{\omega}_c}$ is the filtered progress variable reaction rate. The RHS terms of

Eq. (18) are computed from Filtered Wrinkled Flamelets (FWF) introduced in Section 3. The filtered chemical source term is directly estimated from Eq. (11) as:

$$\overline{\dot{\omega}_c} = \int_{-\infty}^{+\infty} F_\Delta^{1D}(x-x')\overline{\dot{\omega}_c^{*y}}(x')dx' \,, \tag{19}$$

where the superscript * represents the values extracted from the manufactured wrinkled flamelet. The filtered molecular diffusion term is closed as $\overline{\rho \mathbf{V_c}} = -D_m \nabla \tilde{c}$ where D_m is estimated from the manufactured wrinkled flamelet as:

$$D_m = -\overline{\rho^* \mathbf{V_c}^*}/\nabla \tilde{c}^* \,. \tag{20}$$

The sub-filter scale convection term $\nabla \cdot \overline{\rho}(\tilde{c}\tilde{\mathbf{u}} - \widetilde{c\mathbf{u}})$ is modeled as:

$$\mathcal{T} = \nabla \cdot \overline{\rho}(\tilde{c}\tilde{\mathbf{u}} - \widetilde{c\mathbf{u}}) = \rho_0 S_\Delta \left(|\nabla \tilde{c}^*| - |\nabla \overline{c}^*| \right), \tag{21}$$

where ρ_0 and S_Δ are respectively the fresh gas density and consumption speed of the manufactured flamelet filtered at Δ computed from Eq. (12). This formulation ensures that the filtered progress variable iso-surfaces propagate at S_Δ as shown in [10]. For a fixed value of n_Δ, the terms D_m, $\mathcal{T}$ and $\overline{\dot{\omega}_c}$ are pre-computed and tabulated as functions of the filtered progress variable $\tilde{c}$, the flame filter size Δ and the wrinkling factor Ξ_Δ according to Eq. (17). The flame filter size is chosen to ensure that the filtered flame front is well resolved on the LES grid [29,33]. The wrinkling factor can be estimated from the LES using either a transport equation [34], algebraic models [12,15–17] or dynamical formulations [18–20]. The filtered progress variable transport equation closed with tabulated Filtered Wrinkled Flamelets therefore reads:

$$\begin{aligned} \frac{\partial \overline{\rho}\tilde{c}}{\partial t} + \nabla \cdot \overline{\rho}\tilde{c}\tilde{\mathbf{u}} = \nabla \cdot \left(D_m[\tilde{c}, \Delta, \Xi_\Delta]_{n_\Delta} \nabla \tilde{c} \right) \\ + \mathcal{T}[\tilde{c}, \Delta, \Xi_\Delta]_{n_\Delta} + \overline{\dot{\omega}_c}[\tilde{c}, \Delta, \Xi_\Delta]_{n_\Delta} \,. \end{aligned} \tag{22}$$

This modeling strategy is similar to the F-TACLES model [10] except that Filtered Wrinkled Flamelets (FWF) are used instead of Filtered Planar Flamelets (FPF). Therefore, the wrinkling factor Ξ_Δ becomes a coordinate of the FWF database - which integrates the impact of wrinkling on the filtered flame features - instead of multiplying the RHS terms of Eq. (22).

5.3. Estimation of the wavelength parameter n_Δ

The FWF framework assumes that representing the sub-filter scale flame wrinkling with a unique wavelength L_y is sufficient to capture the correct filtered chemical species distribution at the sub-filter scale. This hypothesis will be assessed using *a priori* and *a posteriori* analysis in Sections 6 and 7, respectively. In the context of realistic multi-scale flame wrinkling, the wavelength parameter $n_\Delta = \Delta/L_y$ represents the average number of flame crossings per filter length Δ [35]. Assuming an infinitely thin flame front, Bray et al. [35] show that n_Δ reads :

$$n_\Delta = \frac{\Sigma_\Delta |\overline{\sigma_y}| \Delta}{2} \tag{23}$$

where Σ_Δ is the sub-filter flame surface density which expresses $\Sigma_\Delta = \overline{|\nabla c|} = \Xi_\Delta |\nabla \overline{c}|$. $\overline{\sigma_y}$ is the mean cosine angle of the instantaneous flame front with the $\tilde{c} = c_0$ iso-surface and is assumed to be an universal constant [35,36] so that $|\overline{\sigma_y}| \approx 0.5$. Equation (23) may also be recast as:

$$n_\Delta = C \Delta \Xi_\Delta |\nabla(\overline{\rho}\tilde{c})| \tag{24}$$

where $C = 0.25/\rho_b$ with ρ_b is the burnt gases density. In this model formulation given by Eq. (24), n_Δ is not a free parameter as it is related to $\nabla(\overline{\rho}\tilde{c})$ computed from the LES as well as Δ and Ξ_Δ, which are also two FWF table coordinates. In the following, $\overline{\rho}\tilde{c}$ will be computed directly from the DNS database in the *a priori* analysis (Section 6) whereas it will be transported following Eq. (18) in the *a posteriori* analysis (Section 7).

5.4. Synoptic of FWF model workflow

Given an LES grid and burner operating conditions, the step-by-step procedure to generate a FWF table and use it in a turbulent premixed flame LES is summarized here:

1. Compute the 1-D premixed flame at selected operating conditions using detailed chemistry.
2. Based on the computed 1-D flame, generate a series of 2-D wrinkled flamelets varying sine amplitude A and wavelength n_Δ as detailed in Section 3.1. Knowing the grid cell size Δx, the suggested flame filter size is $\Delta = 5\Delta x$.
3. Filter the different mapped variables to compute $\widetilde{rT}$, $\widetilde{T}$, $\widetilde{Y_k}$, $\overline{\dot{\omega}_{Y_k}}$, D_m, $\mathcal{T}$, $\overline{\dot{\omega}_c}$.
4. Tabulate these variables as $\overline{\Phi} = \overline{\Phi}[\tilde{c}, \Delta, \Xi_\Delta]_{n_\Delta}$
5. Perform the LES using $\widetilde{rT}$ to close the equation of state. The filtered progress variable equation is closed using D_m and $\mathcal{T} + \overline{\dot{\omega}_c}$ as diffusion term and reaction rate, respectively. Other optional quantities such as $\widetilde{Y_k}$ and $\overline{\dot{\omega}_{Y_k}}$ can be accessed as post-processing variables.

The implementation of the FWF model and its tabulation procedure are validated by computing a series of 1-D filtered CH_4-air flames at $\phi = 0.83$ for different filter sizes Δ. In these 1-D simulations, Eq. (22) is solved by assuming constant values of the sub-filter scale wrinkling Ξ_Δ. They are performed to verify that the filtered flame front effectively propagates at $S_\Delta = \Xi_\Delta S_l^0$ whatever the choice of the flame pattern parameter n_Δ. The simulation results, not detailed here, showed that the resolution criterion $\Delta/\Delta_x \geq 5$ was needed to ensure an error of less than 3% on S_Δ. This conclusion was also drawn for other filtered flame models implemented in the YALES2 code [10,29].

6. A priori comparison of FWF distributions against a filtered DNS database

An *a priori* validation of the methodology is performed by challenging the Filtered Density Function (FDF) reconstructed using FWF against the DNS data [11,30] introduced in Section 2. Reference progress variable FDF are extracted from the PRECCINSTA database by using the procedure detailed in [11] and plotted in Fig. 12 for different pairs $(\tilde{c}, S_c)$, where S_c, the unmixedness factor, reads $S_c = \widetilde{c''^2}/(\tilde{c}(1-\tilde{c}))$ and two filter size $\Delta/\delta_l^0 = 2$ and $\Delta/\delta_l^0 = 4$.

The FWF sub-filter FDF is computed by first recasting Eq. (10) as follows:

$$\overline{\rho}\widetilde{\Phi} = \int_0^1 \int_{-\infty}^{+\infty} \frac{F_\Delta^{1D}(x-x')}{L_y} \left[\int_{-L_y/2}^{+L_y/2} \rho \Phi \delta(c - \mathcal{C}) dy' \right] dx' d\mathcal{C} \tag{25}$$

where $\rho = \rho(x', y')$, $c = c(x', y')$ and δ is the dirac distribution. Then, a statistical expression of $\widetilde{\Phi}$ is obtained by introducing $\widetilde{P}^{\mathrm{FWF}}$, the FDF associated to FWF:

$$\widetilde{\Phi} = \int_0^1 \Phi \widetilde{P}^{\mathrm{FWF}}(\mathcal{C}) d\mathcal{C} \tag{26}$$

where

$$\widetilde{P}^{\mathrm{FWF}}(\mathcal{C}) = \frac{1}{\overline{\rho}} \int_{-\infty}^{+\infty} \frac{F_\Delta^{1D}(x-x')}{L_y} \left[\int_{-L_y/2}^{+L_y/2} \rho \delta(c - \mathcal{C}) dy' \right] dx' \tag{27}$$

First and second moments of the progress variable are computed from the FWF-FDF as follow:

$$\tilde{c} = \int_0^1 c \widetilde{P}^{\mathrm{FWF}}(\mathcal{C}) d\mathcal{C} \tag{28}$$

$$\widetilde{c''^2} = \int_0^1 (c - \tilde{c})^2 \widetilde{P}^{\mathrm{FWF}}(\mathcal{C}) d\mathcal{C} \tag{29}$$

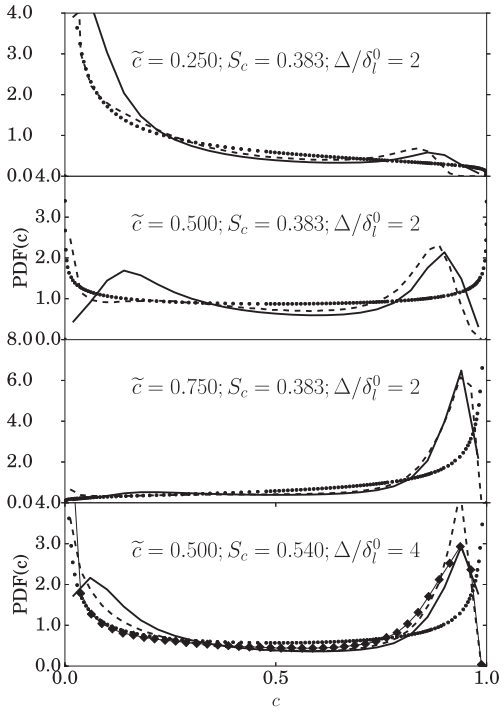

Fig. 12. Comparison of the filtered density function of the progress variable using FWF, the β-distribution (PCM-FPI) and the filtered DNS of the PRECCINSTA burner. Legend: — Filtered DNS, ... β distribution, – – FWF distribution ($n_\Delta = 1$), ♦—♦ FWF distribution ($n_\Delta = 2$).

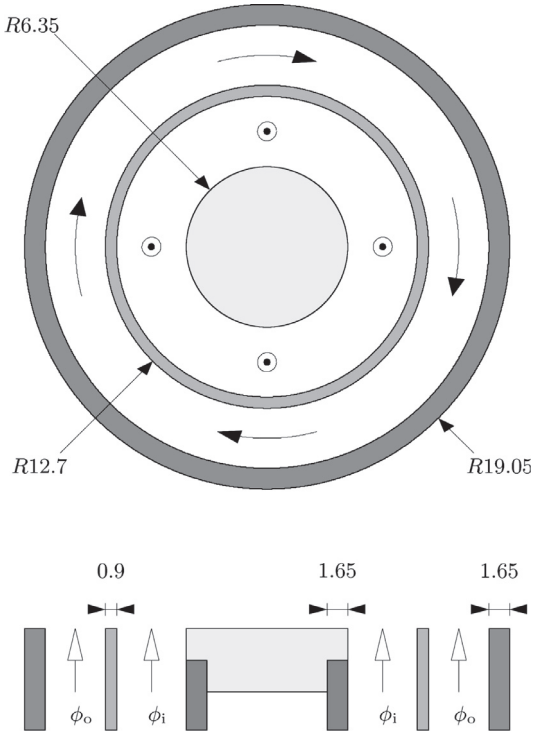

Fig. 13. Scheme representing the Cambridge SwB burner.

$\widetilde{P}^{FWF}(\mathcal{C})$ is numerically pre-computed by using Eq. (27) for two flame patterns at the sub-filter scale ($n_\Delta = 1$ and $n_\Delta = 2$) and by varying the amplitude A across the range of validity defined in Section 3.2. The wrinkled flame patterns are generated from a 1-D CH_4-air flame computed at $\phi = 0.83$ using detailed chemistry [28]. The corresponding first and second moments of progress variable are calculated from Eqs. (28) and (29), respectively, so that the FWF-FDF can be added to Fig. 12 for both filter sizes $\Delta = 2\delta_l^0$ and $\Delta = 4\delta_l^0$. Finally, a standard β-distribution parameterized also by $\widetilde{c}$ and S_c and frequently used to couple tabulated chemistry with a statistical description of the turbulence [2,37,38], is also added in Fig. 12 for comparison.

In the cases $\Delta/\delta_l^0 = 2$, the FWF parameter n_Δ is set to 1. This value is obtained from the DNS parameters and the model of Eq. (24). The FWF-PDF retrieves the shape of the reference FDF extracted from the filtered DNS, especially in the burned gases where the results are better than the β-distribution. However, the model is less accurate on the unburned gases side and behaves as the β-distribution. This behavior was also found in other filtered flame models [11] and was attributed to a lack of intermittency on the unburnt gases side. Indeed, no turbulent mixing is taken into account on the unburned gas side in the FWF model, i.e. the progress variable iso-lines in the preheat zone tend to follow the imposed flame shape. The only differences between the $c = c_0$ iso-line and the other iso-values are due to curvature effects, which lead to a decrease of the iso-line wrinkling away from the flame front. As a result, when the flame thickness is less than the filter size, the model promotes values close to $c = 0$. In the DNS, intermediate values of c in the pre-heat zone are more present in the sub-filter volume due to the gradient transport created by the turbulent mixing. This effect is not present on the burnt gas side, as the level of turbulence intensity is largely attenuated by the increase of the molecular viscosity and the filtered flame shape is recovered. Additionally, this figure enables to illustrate the influence of the n_Δ parameter. When n_Δ increases, the flame front pattern amplitude decreases for the same wrinkling value and the progress variable iso-lines in the vicinity of the flame front become flatter. Then, their probability of being in the sub-filter volume decreases as their wrinkling decreases. This effect is compensated by a slight increase of the other PDF values close to the $c = c_0$ level and at $c = 0$ and $c = 1$.

7. Application of the FWF model to a turbulent premixed flame

7.1. Experimental configuration and numerical set-up

The Cambridge stratified swirled burner (SwB) [39], represented in Fig. 13, is retained for challenging the FWF model. It consists in a central bluff body surrounded by two annular channels in which premixed fuel/air mixtures are injected. Velocities in the inner and outer channels are respectively $U_i = 8.31$ m.s^{-1} and $U_o = 18.7$ m.s^{-1}, giving rise to strong shear layers. A co-flow of air with velocity $U_{cf} = 0.4$ m.s^{-1} is set to avoid entrainment effects. The burner has been studied for different levels of stratification and swirl numbers. An important experimental database includes velocity [40–42] as well as temperature, chemical species and equivalence ratio measurements [40,41,43]. Burner walls temperatures have been characterized by [44] and a particular focus on the differential diffusion effects has been made in [45]. More recently, an experimental analysis performed in [46,47] has shown that the inner chemical flame structure of non-swirling and swirling SwB flames remains very close to laminar flame structure which is in line with the flamelet assumption made by the FWF formulation.

Numerical studies previously published mainly focused on the non-swirling premixed and stratified configurations [48–54] for which differential diffusion and heat losses at the bluff-body play an important role on the turbulent flame structure [52] and pollutants formation [53,54]. However, very few investigations have been conducted on the swirling cases using LES [55]. In the present work, the premixed highly swirling flame SwB3 is considered. The

Table 1
Discretization of the FWF table. The file size obtained for this table is 93MB.

Coordinate	# of points	Min	Max
C	300	0.0	1.0
Ξ_Δ	7	1.0	4.0
Δ	2	1.25 mm	2.5 mm
Z	16	0.0	1.0
n_Δ	4	1.0	4.0

equivalence ratios of inner and outer streams are $\phi_i = \phi_o = 0.75$. The swirl number[1] is estimated experimentally [41] to $S = 0.79$. A lower influence of differential diffusion has been observed experimentally in highly swirling cases and is attributed to a significant change in the recirculation zone compared to non-swirling cases. LES simulation of this configuration has been conducted by [55] using a reduced chemical scheme of 19 species and 15 reactions coupled to a transported PDF closure. Although adiabatic walls and unity Lewis number were assumed, very good agreement of temperature and species mass fractions profiles were obtained except for the burnt gases located within the inner recirculation zone.

The low-Mach number LES solver YALES2 [56] for unstructured grids is retained in this study. It features a central fourth-order scheme for spatial discretization while time integration of convective terms is performed with an explicit fourth-order temporal scheme. The simulations of the SwB3 flame are performed on two tetrahedral grids. The coarse grid contains $17 \cdot 10^6$ nodes with a resolution $\Delta_x = 0.5$ mm in the injection tube and flame region. The fine grid is an homogeneous refinement of the coarse one and features $135 \cdot 10^6$ nodes with a resolution $\Delta_x = 0.25$ mm.

An FWF table has been generated from a collection of CH_4-air 1-D flames computed at different equivalence ratios going from $\phi_l = 0.5$ to $\phi_r = 4.0$. A linear prolongation is performed to pure air and pure CH_4 except for source terms which are set to 0 out of the flammability limits. The iso-line $c = c_0 = 0.8$ chosen to generate the FWF pattern corresponds to the maximum value of the heat release rate. Table coordinates and file size are detailed in Table 1.

The FWF filter sizes are $\Delta = 5 \times \Delta_x = 2.5$ mm for the coarse mesh and $\Delta = 5 \times \Delta_x = 1.25$ mm for the fine mesh. For the burner operating equivalence ratio, $\Phi = 0.75$, the ratio Δ/δ_l^0 equals 4.8 and 2.4, for coarse and fine meshes, respectively. The flame filter size is here chosen so that the filtered flame front is well resolved on a given mesh of size Δ_x when there is no subgrid scale flame wrinkling, as in the original F-TACLES formulation [10]. Figure 6 shows however that the filtered flame wrinkling thickness, and consequently the filtered reactive layer [33], increases with Ξ_Δ. An optimization, not done in the present work, would be to correlate the flame filter size to Δ_x but also to n_Δ and Ξ_Δ.

Sub-filter scale flame wrinkling is modeled using a fractal-like formulation [18,20,57,58] for the wrinkling factor:

$$\Xi_\Delta = \left(\Delta/\delta_l^0\right)^\beta \tag{30}$$

with a dynamic estimation of the fractal-like parameter β which varies in space and time such as $\beta \in [0, 1]$. Therefore, the maximum value of wrinkling $\Xi_\Delta^{\max}$ for a given mesh is known *a priori* and allows to choose properly the maximum value of the Ξ_Δ coordinate so that $\Xi_\Delta^{\max} = \Delta^{\max}/\delta_l^{0\,\min}$. The n_Δ extrema is undetermined at the table generation stage as it depends on resolved LES quantities, accordingly to Eq. (24). The chemical filtered table

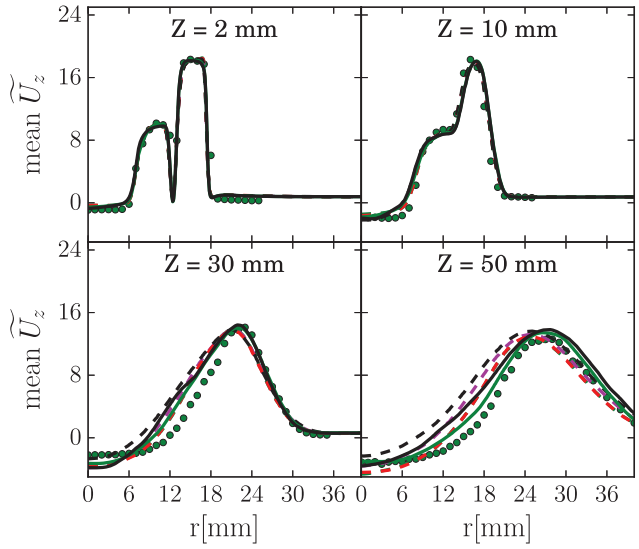

Fig. 14. 1-D radial profiles of the mean axial velocity U_z at different distances Z from the bluff-body wall surface. Legend: 17M-FWF-N1, 17M-FWF-N3, 17M-FWF-NM, 17M-FPF, 135M-FWF-N1, 135M-FPF, Experiments.

is here build-up for n_Δ ranging between 1 and 4, which will *a posteriori* confirmed by the LES.

The different simulations performed in this study are listed in Table 2. The first simulations are performed on the coarse mesh to estimate the impact of the n_Δ parameter especially on the prediction of CO filtered mass fraction. Two simulations are conducted with the constant values $n_\Delta = 1$ (17M-FWF-N1) and $n_\Delta = 3$ (17M-FWF-N3). A third simulation (17M-FWF-NM) is performed using the model proposed in Eq. (24). The last coarse mesh simulation (17M-FPF) is performed using the original F-TACLES model [10] which assumes Filtered Planar Flamelet (FPF) at the sub-filter scale. Two simulations are then conducted on the fine mesh and correspond to the homogeneous mesh refinement of the F-TACLES model simulation (135M-FPF) and to the FWF model simulation (135M-FWF-N1) with the constant value $n_\Delta = 1$.

7.2. Results analysis

Flow field statistics obtained from the simulation of the swirled premixed burner are shown in Figs. 14–19. A very good agreement is obtained on the first mean and RMS profiles at the burner exit (Z = 2 mm) and validate the inlet boundary conditions against measurements for all the simulations listed in Table 2. This conclusion is verified for the three velocity components: the axial component U_z (Figs. 14 and 15); the orthoradial component U_t (Figs. 16 and 17) and the radial component U_r (Figs. 18 and 19). Going further downstream, the mean and RMS velocity profiles remain in very good agreement with experiments and all the simulations show identical behavior. In particular, the radial shift of the flow due to thermal expansion of burnt gases is well captured by the current modeling strategy.

Mean and RMS profiles of flame temperature profiles are shown in Figs. 20 and 21, respectively, for axial positions[2] z = 10 mm, z = 30 mm, z = 40 mm and z = 50 mm. In this burner configuration, temperature profiles allow to clearly identify the flame brush. Focusing on the coarse mesh simulations in dashed lines (17M-FWF-N1; 17M-FWF-N3; 17M-FWF-NM; 17M-FPF), the position of

[1] The swirl number is defined as $S = U_{tg}/U_z$ where U_{tg} and U_z are the mean tangential and axial velocities above the center of the outer annulus [41].

[2] Note that axial positions selected for temperature and chemical species comparisons are different from the ones selected for velocity profiles comparisons because experimental datasets are not available at the same locations.

Table 2
Summary of the different simulations.

Name	Δ_x	Model	n_Δ	Legend
17M-FWF-N1	0.5 mm	Filtered Wrinkled Flamelet	1.0	- - -
17M-FWF-N3	0.5 mm	Filtered Wrinkled Flamelet	3.0	- - -
17M-FWF-NM	0.5 mm	Filtered Wrinkled Flamelet	Eq. (24)	- - -
17M-FPF	0.5 mm	Filtered Planar Flamelet [10]	–	- - -
135M-FWF-N1	0.25 mm	Filtered Wrinkled Flamelet	1.0	—
135M-FPF	0.25 mm	Filtered Planar Flamelet [10]	–	—

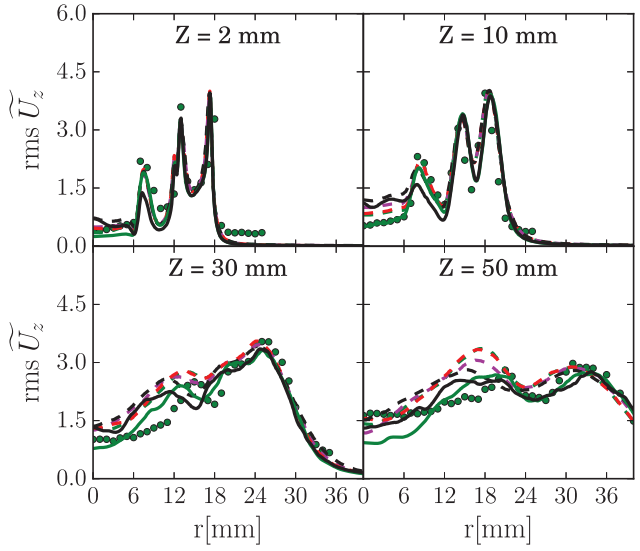

Fig. 15. 1-D radial profiles of the RMS of axial velocity U_z at different distances Z from the bluff-body wall surface. Legend: - - - 17M-FWF-N1, - - - 17M-FWF-N3, - - - 17M-FWF-NM, - - - 17M-FPF, — 135M-FWF-N1,— 135M-FPF, ● ● Experiments.

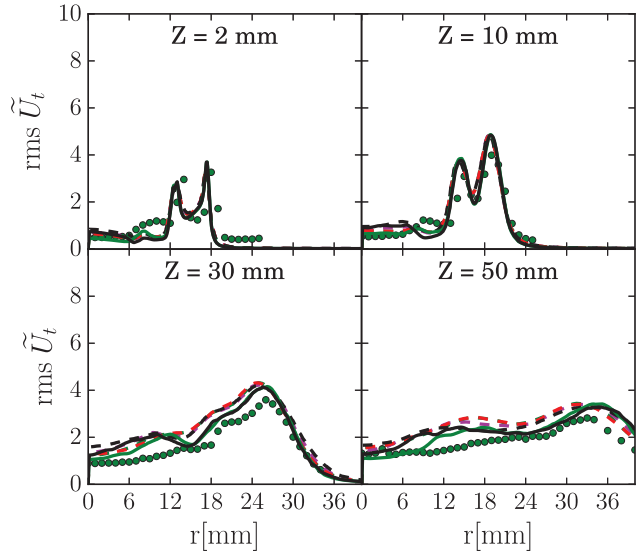

Fig. 17. 1-D radial profiles of the RMS of orthoradial velocity U_t at different distances Z from the bluff-body wall surface. Legend: - - - 17M-FWF-N1, - - - 17M-FWF-N3, - - - 17M-FWF-NM,- - - 17M-FPF, — 135M-FWF-N1,— 135M-FPF, ● ● Experiments.

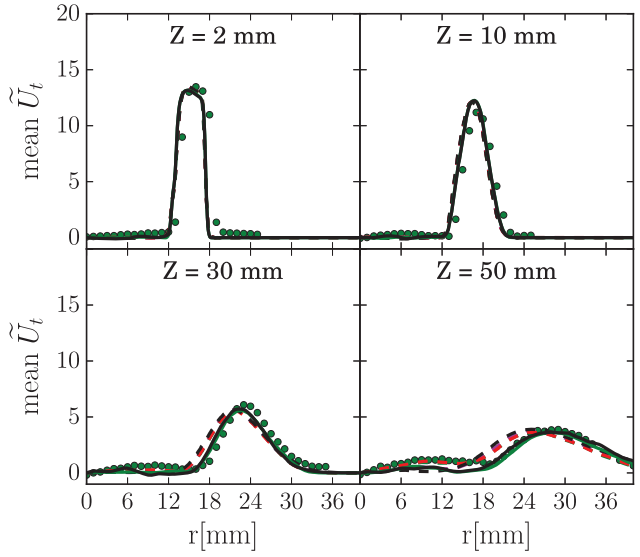

Fig. 16. 1-D radial profiles of the mean orthoradial velocity U_t at different distances Z from the bluff-body wall surface. Legend: - - - 17M-FWF-N1, - - - 17M-FWF-N3, - - - 17M-FWF-NM, - - - 17M-FPF, — 135M-FWF-N1,— 135M-FPF, ● ● Experiments.

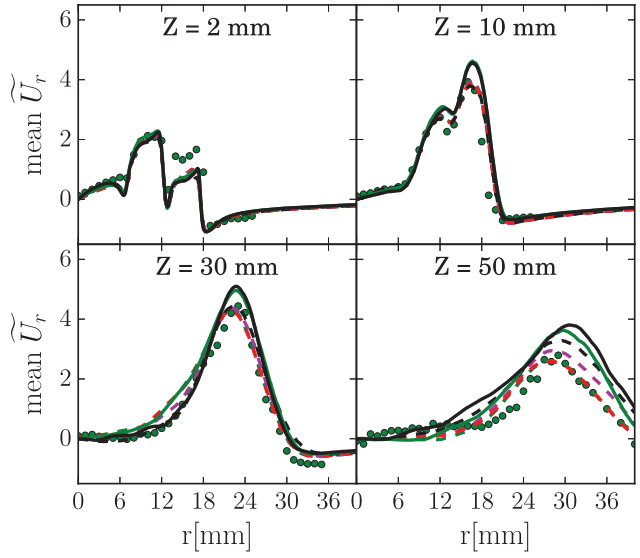

Fig. 18. 1-D radial profiles of the mean radial velocity U_r at different distances Z from the bluff-body wall surface. Legend: - - - 17M-FWF-N1, - - - 17M-FWF-N3, - - - 17M-FWF-NM,- - - 17M-FPF, — 135M-FWF-N1,— 135M-FPF, ● ● Experiments.

the mean flame brush is accurately predicted on the first positions while a slight shift is observed further downstream for Z = 40 mm and Z = 50 mm. This slight shift is also confirmed by RMS comparisons but does not seem to depend on the combustion model. Figure 22a shows an instantaneous iso-surface of the progress variable reaction rate $\overline{\dot{\omega}_c}$ colored by the value of the fractal parameter $\beta \in [0, 1]$ of the wrinkling model for Ξ_Δ. 2-D cut of the instantaneous field of Ξ_Δ is also available in Fig. 22b (right). A very large range of variation of β is observed and two main zones can be identified in the flame: (i) the near burner region where the flame has a low wrinkling characterized by $\beta \approx 0$ (*i.e.* $\Xi_\Delta \approx 1$); (ii) further downstream where the flame crosses the shear layer holding

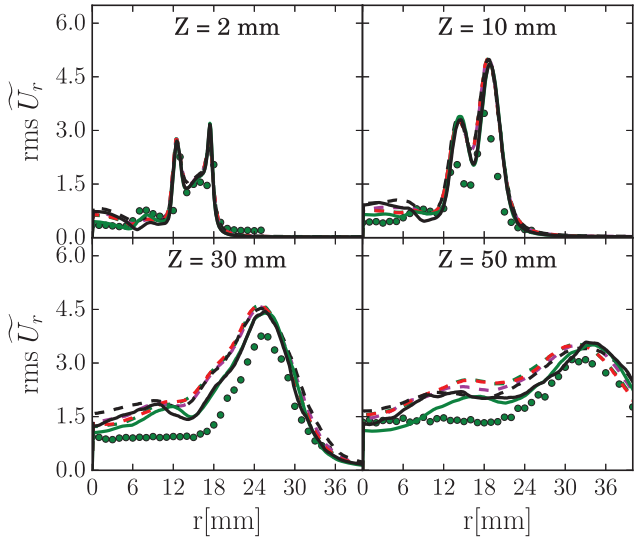

Fig. 19. 1-D radial profiles of the RMS of radial velocity U_r at different distances Z from the bluff-body wall surface. Legend: 17M-FWF-N1, 17M-FWF-N3, 17M-FWF-NM, 17M-FPF, 135M-FWF-N1, 135M-FPF, Experiments.

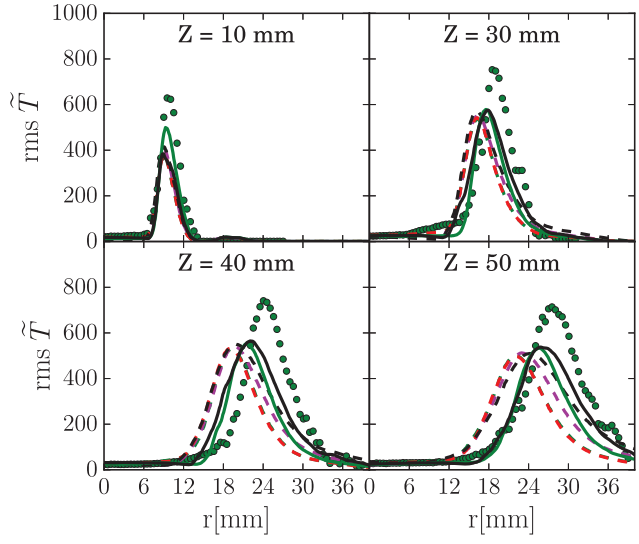

Fig. 21. 1-D radial profiles of the RMS of temperature at different distances Z from the bluff-body wall surface. Legend: 17M-FWF-N1, 17M-FWF-N3, 17M-FWF-NM, 17M-FPF, 135M-FWF-N1, 135M-FPF, Experiments.

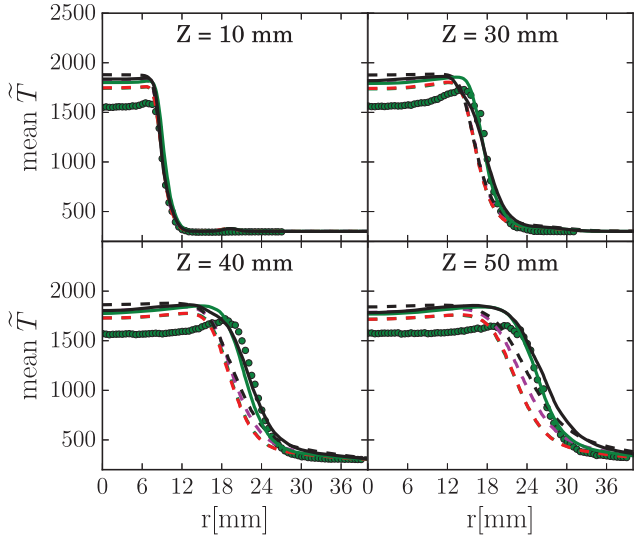

Fig. 20. 1-D radial profiles of the mean temperature at different distances Z from the bluff-body wall surface. Legend: 17M-FWF-N1, 17M-FWF-N3, 17M-FWF-NM, 17M-FPF, 135M-FWF-N1, 135M-FPF, Experiments.

between inner and outer tubes and becomes highly wrinkled with β reaching values close to 1. As discussed in [52] for non-swirling cases, this configuration is very challenging for the sub-filter scale wrinkling model. Assuming that the level of resolved wrinkling was not sufficient to obtain a correct estimation of the β parameter, two other simulations are conducted on the refined mesh (135M-FWF-N1 and 135M-FPF). Results of these simulations are showed in full lines in both velocity profiles (Figs. 14–19) and temperature profiles (Figs. 20 and 21). Even though no significant modification of the mean and RMS velocity profiles are observed, the mean flame position better compares with experimental data for all the considered axial positions. The same behavior is noted both for FPF (135M-FPF) and FWF (135M-FWF-N1) models and is also confirmed by RMS profiles. The slight misprediction of the flame brush far from the burner exit can be attributed to the sub-filter scale wrinkling modeling and seems to be independent from the combustion models considered here.

An important discrepancy is observed between measured and simulated burnt gases temperature. This discrepancy is not dependent from the mesh resolution and is found for both FWF and FPF models. Precedent studies on non-swirling cases [52–54] indicate that such discrepancies may be due to both differential diffusion and/or non-adiabaticity effects which are not included in the present simulations. The inclusion of such effects within the FWF framework will be considered in future work. Therefore, detailed investigations for the present SwB3 case are out of the scope of the present study.

The ability of the new modeling strategy for predicting pollutants is assessed by comparing simulated and experimental CH_4 and CO mass fractions. The mean profiles of chemical mass fractions are plotted in Fig. 23 for CH_4 and Fig. 24 for CO. Focusing on the CH_4 mass fraction profiles, a behavior very similar to temperature profiles is retrieved. The mean values are in a very good agreement with experimental results and a slight shift of the profiles (17M-FWF-N1; 17M-FWF-N3; 17M-FWF-NM; 17M-FPF) is observed only for coarse mesh. The three FWF simulations on the coarse mesh give the same prediction in terms of mean flame position, flame brush thickness and mean CH_4 value suggesting that the n_Δ parameter has a negligible impact as for temperature and velocity. Figure 22b shows 2-D cut of the instantaneous field of n_Δ for the 17M-FWF-NM case. It appears that the model predicts a nearly constant value of $n_\Delta \approx 1$ explaining the similarity of both 17M-FWF-N1 and 17M-FWF-NM simulation results. Since the simulation with planar flamelets at the sub-filter scale (17M-FPF) also gives very similar results, the effect of the sub-filter scale wrinkling on the CH_4 predictions also has a negligible influence. In this case, the CH_4 mass fraction in the direction normal to the instantaneous flame front is strictly decreasing. For such major chemical species and in the case of realistic ratio $\Delta/\delta_l^0 \gg 1$, mean values are mainly controlled by the intermittency between fresh and burnt gases. The contribution of the sub-filter scale wrinkling of the filtered profiles are weak. This is also true for temperature profiles as discussed in the *a priori* study in Sec. 2 and confirmed by Figs. 20 and 21.

The focus is now made on CO mass fraction profiles shown in Fig. 24 and representative of intermediate species not present in fresh and burnt gases. Two coarse mesh simulations with the constant values $n_\Delta = 1$ (17M-FWF-N1) and $n_\Delta = 3$ (17M-FWF-N3) are shown and a third simulation (17M-FWF-NM) uses the model

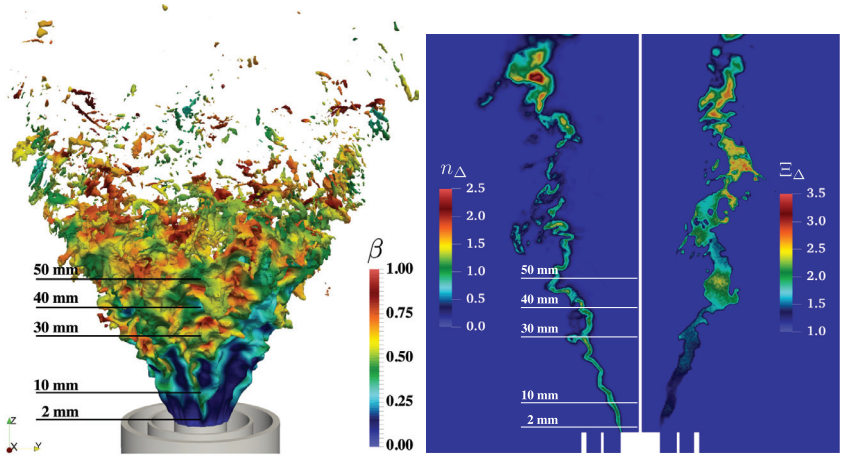

(a) Isosurface $\overline{\omega_c} = \max(\overline{\omega_c})/2$ colored by the fractal parameter β.

(b) 2-D cut of n_Δ (left) and Ξ_Δ (right) scalar fields.

Fig. 22. Instantaneous views of the SWB3 flame (17M-FWF-NM) with the indication of the radial profiles axial positions.

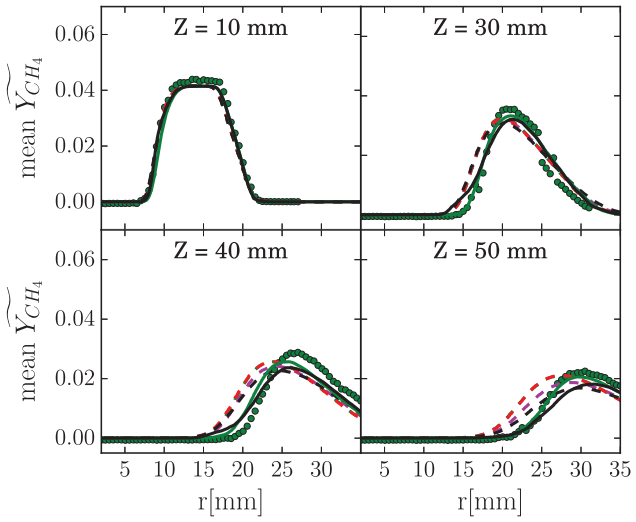

Fig. 23. 1-D radial profiles of the mean CH_4 mass fraction at different distances Z from the bluff-body wall surface. Legend: - - - 17M-FWF-N1, - - - 17M-FWF-N3, - - - 17M-FWF-NM,- - - 17M-FPF, ___ 135M-FWF-N1, — 135M-FPF, ● ● Experiments.

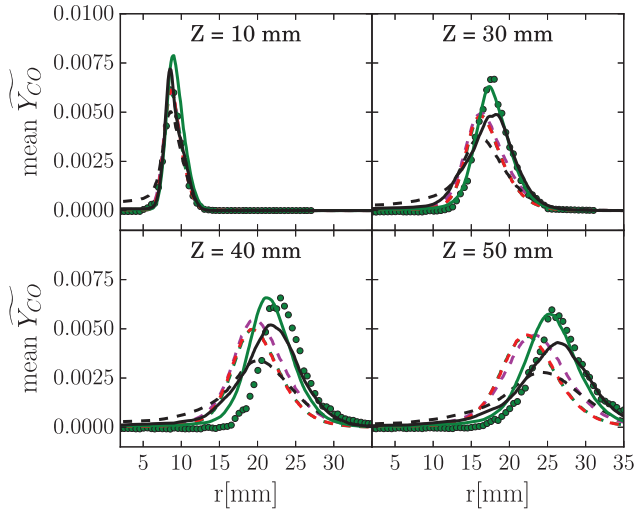

Fig. 24. 1-D radial profiles of the mean CO mass fraction at different distances Z from the bluff-body wall surface. Legend: - - - 17M-FWF-N1, - - - 17M-FWF-N3, - - - 17M-FWF-NM, - - - 17M-FPF, ___ 135M-FWF-N1, — 135M-FPF, ● ● Experiments.

proposed in Eq. (24). As shown in Fig. 22b and discussed previously, 17M-FWF-NM predicts a nearly constant value of $n_\Delta \approx 1$ and therefore behaves close to 17M-FWF-N1 simulation. Additionally, no differences are observed between 17M-FWF-N1 and 17M-FWF-N3 cases showing that the impact of n_Δ on filtered species mass fractions remains negligible in this case even for intermediate species. This observation is in line with the *a priori* analysis conducted in Section 3.4 (Fig. 8) especially for the ratio $\Delta/\delta_l^0 \approx 5$ of the simulated cases.

The refined FWF simulation has been conducted only for $n_\Delta = 1$ (135M-FWF-N1) because of the smaller impact of n_Δ expected for lower ratio Δ/δ_l^0. A greater impact of n_Δ may be found for less resolved LES or higher operating pressures (*i.e.* smaller laminar flame thickness). This motivates the choice to keep n_Δ as a parameter of the model even if its impact is negligible in the present study. Predictions using FPF (17M-FPF) is slightly below FWF (17M-FWF) near the flame basis (Z = 10 mm) where the sub-filter scale wrinkling is low. At this location, the flame brush is thin and compares with flame thickness. In this particular case, it is expected that the equivalent filtering volume of measurements is not negligible compare to the flame brush and may lower the real maximum value of the experiments [59] as observed here. The differences of CO mean values increase further downstream where the SGS wrinkling increases and FWF keeps better predicting CO levels. At axial positions Z = 40 mm and Z = 50 mm, a strong influence of the model is indeed observed. Adding the wrinkling factor as a supplementary table coordinate enables an accurate prediction of CO in the flame brush regions. A similar conclusion has been obtained in a Reynolds-Averaged Navier-Stokes (RANS) context by [60] where a turbulent premixed flame was computed using a level-set G-equation model coupled to a flamelet library model of Peters [32]. The impact of flame wrinkling on CO profiles was accounted for by rescaling length scale coordinate (*i.e.* the mean distance function G) and was compulsory to retrieve correct mean CO profiles against experiments. This conclusion is also confirmed by the comparison of FPF (135M-FPF) and FWF (135M-FWF-N1) refined mesh simulations where the same behavior is reproduced. As excepted, a lower discrepancy between the refined

mesh predictions of both models is observed since the ratio Δ/δ_l^0 (and therefore the level of unresolved wrinkling) is twice lower.

8. Conclusion

A new methodology is proposed to analyze and capture the impact of the flame wrinkling at the sub-filter scale. A progress variable iso-line is assumed sinusoidal in a 2-D plane and parametrized by its wavelength $L_y = \Delta/n_\Delta$ and its amplitude A. The distance function from this iso-line is then used to reconstruct a 2-D wrinkled flamelet from the thermochemical structure of a 1-D premixed flame computed with detailed chemistry. The FWF model estimates the unclosed terms of the filtered progress variable equation by explicitly filtering this 2-D wrinkled flame for different filter sizes Δ, different wrinkling levels Ξ_Δ and different wavelength parameters n_Δ. The model is implemented and validated in both *a priori* and *a posteriori* analysis. A priori comparison is conducted in the statistical formalism and shows a good behavior of the FWF Filtered Density Function when compared to a filtered DNS database. FWF model is then applied to the turbulent premixed and swirling flame SwB3 stabilized behind a bluff-body. A very good agreement of velocity, temperature and species mass fraction profiles is obtained against experiments. FWF results are also compared to the original F-TACLES formulation which does not account for the impact of sub-filter scale wrinkling on the filtered flame structure (assumed planar). A clear improvement of the intermediate species mass fraction prediction is observed.. The prediction of major species and temperature profiles are identical for both models. In the other hand, the influence of the wavelength parameter n_Δ is found negligible in this configuration for which $\Delta/\delta_l^0 \approx 5$. These results show that, for a given sub-filter scale wrinkling Ξ_Δ, accounting for the impact of the wrinkling on filtered intermediate chemical species is of primary importance while geometrical details of the wrinkled flame pattern at the sub-filter scale are of lower importance. However, accounting for sub-filter scale wrinkling on filtered flame structure to predict only major species and temperature appears to be unnecessary. It means that the model has a strong passive impact on the species post-processing but a slight active impact on the progress variable source term and on the flame heat release. The main limitation of the proposed modeling approach is the flamelet assumption associated to tabulated chemistry. Therefore, the extension to other combustion regimes (thin reaction zone), mixing regimes (partially-premixed, diffusion) and especially multi-regime cases may be difficult. Future work will explore the coupling of FWF model with transported chemistry which may help to generalize the present approach.

Finally, the gain of the method depends on the quantity of interest. Benefit remain low in steady flame situations where equilibrium is reached at the combustion chamber exit. Standard filtered or thickened flamelet-based models are indeed able to provide equilibrium species mass fluxes. Benefit are however higher in configurations where the flame is sensitive to unsteady phenomena such as local extinction, as for instance in emerging low-temperature combustors. In such situations, as products does not necessarily reach equilibrium at the exit of the chamber, an accurate prediction of the local mass of species is mandatory. Here the effort has been made on CO as experimental measurements were available but the overall methodology is of interest for predicting other pollutant species such as for instance NOx or soot precursors.

Acknowledgements

We thank Prof. Simone Hochgreb for providing experimental data. This work was granted access to the HPC resources from IDRIS, TGCC and CINES under the allocation x2015-2b6880 made by GENCI (Grand Equipement National de Calcul Intensif) and from CRIHAN (Centre de Ressources Informatiques de Haute-Normandie) under the allocation 2012–006.

References

[1] S.B. Pope, Small scales, many species and the manifold challenges of turbulent combustion, Proc. Combust. Inst. 34 (1) (2013) 1–31.
[2] B. Fiorina, D. Veynante, S. Candel, Modeling combustion chemistry in large eddy simulation of turbulent flames, Flow Turbulence Combust. 94 (1) (2015) 3–42.
[3] T. Poinsot, D. Veynante, Theoretical and numerical combustion, third, 2012.
[4] H. Pitsch, Large eddy simulation of turbulent combustion, Annu. Rev. Fluid. Mech. 38 (2006) 453–482.
[5] V. Moureau, B. Fiorina, H. Pitsch, A level set formulation for premixed combustion LES considering the turbulent flame structure, Combust Flame 156 (4) (2009) 801–812.
[6] E. Knudsen, S.H. Kim, H. Pitsch, An analysis of premixed flamelet models for large eddy simulation of turbulent combustion, Phys. Fluids 22 (11) (2010) 115109-1–115109-24.
[7] E. Knudsen, H. Kolla, E.R. Hawkes, H. Pitsch, LES of a premixed jet flame DNS using a strained flamelet model, Combust. Flame 160 (12) (2013) 2911–2927.
[8] M. Boger, D. Veynante, H. Boughanem, A. Trouvé, Direct numerical simulation analysis of flame surface density concept for large eddy simulation of turbulent premixed combustion, Proc. Combust. Inst. 27 (1) (1998) 917–925.
[9] C. Duwig, Study of a filtered flamelet formulation for large eddy simulation of premixed turbulent flames, Flow Turbul. Combust. 79 (4) (2007) 433–454.
[10] B. Fiorina, R. Vicquelin, P. Auzillon, N. Darabiha, O. Gicquel, D. Veynante, A filtered tabulated chemistry model for LES of premixed combustion, Combust. Flame 157 (3) (2010) 465–475.
[11] V. Moureau, P. Domingo, L. Vervisch, From large-eddy simulation to direct numerical simulation of a lean premixed swirl flame: Filtered laminar flame-PDF modeling, Combust. Flame 158 (7) (2011) 1340–1357.
[12] O. Colin, F. Ducros, D. Veynante, T. Poinsot, A thickened flame model for large eddy simulations of turbulent premixed combustion, Phys. Fluids 12 (7) (2000) 1843–1863.
[13] G. Kuenne, A. Ketelheun, J. Janicka, LES modeling of premixed combustion using a thickened flame approach coupled with FGM tabulated chemistry, Combust. Flame 158 (2011) 1750–1767.
[14] G. Kuenne, A. Avdic, J. Janicka, Assessment of subgrid interpolation for the source term evaluation within premixed combustion simulations 178 (2017) 225–256.
[15] F. Charlette, C. Meneveau, D. Veynante, A power-law flame wrinkling model for LES of premixed turbulent combustion, part i: non-dynamic formulation, Combust. Flame 131 (1/2) (2002) 159–180.
[16] H. Pitsch, A consistent level set formulation for large-eddy simulation of premixed turbulent combustion, Combust. Flame 143 (4) (2005) 587–598.
[17] C. Fureby, A fractal flame-wrinkling large eddy simulation model for premixed turbulent combustion, Proc. Combust. Inst. 30 (1) (2005) 593–601.
[18] G. Wang, M. Boileau, D. Veynante, Implementation of a dynamic thickened flame model for large eddy simulations of turbulent premixed combustion, Combust. Flame 158 (11) (2011) 2199–2213.
[19] G. Wang, M. Boileau, D. Veynante, K. Truffin, Large eddy simulation of a growing turbulent premixed flame kernel using a dynamic flame surface density model, Combust. Flame 159 (8) (2012) 2742–2754.
[20] T. Schmitt, A. Sadiki, B. Fiorina, D. Veynante, Impact of dynamic wrinkling model on the prediction accuracy using the F-TACLES combustion model in swirling premixed turbulent flames, Proc. Combust. Inst. 34 (1) (2013) 1261–1268.
[21] G. Kuenne, F. Seffrin, F. Fuest, T. Stahler, A. Ketelheun, D. Geyer, J. Janicka, A. Dreizler, Experimental and numerical analysis of a lean premixed stratified burner using 1D Raman/Rayleigh scattering and large eddy simulation, Combust. Flame 159 (8) (2012) 2669–2689.
[22] B. Fiorina, R. Mercier, G. Kuenne, A. Ketelheun, A. Avdic, J. Janicka, D. Geyer, A. Dreizler, E. Alenius, C. Duwig, P. Trisjono, K. Kleinheinz, S. Kang, H. Pitsch, F. Proch, F. Cavallo Marincola, A. Kempf, Challenging modeling strategies for LES of non-adiabatic turbulent stratified combustion, Combust. Flame 162 (11) (2015) 4264–4282.
[23] S. Menon, A.R. Kerstein, Turbulent Combustion Modeling, springer edition, Vol. 95, Fluid Mechanics and Its Applications (2011), pp. 220–248, doi:10.1007/978-94-007-0412-1_9. Ch. the Linear-Eddy Model
[24] L. Vervisch, R. Haugel, P. Domingo, M. Rullaud, Three facets of turbulent combustion modelling: DNS of premixed flame, LES of lifted nonpremixed V-flame and rans of jet-flame, J. Turbul. 5 (4) (2004) 1–36.
[25] D. Haworth, Progress in probability density function methods for turbulent reacting flows, Progr. Energy Combust. Sci. 36 (2) (2010) 168–259, doi:10.1016/j.pecs.2009.09.003.
[26] M.S. Sweeney, S. Hochgreb, M.J. Dunn, R.S. Barlow, A comparative analysis of flame surface density metrics in premixed and stratified flames, Proc. Combust. Inst. 33 (2011) 1419–1427.
[27] N. Darabiha, Transient behaviour of laminar counterflow hydrogen-air diffusion flames with complex chemistry, Combust. Sci. Tech. 86 (1992) 163–181.
[28] P. Lindstedt, 12 month progress report 1, Technical Report, Brite Euram Program Project BRPR950056, 1997.

[29] R. Mercier, V. Moureau, D. Veynante, B. Fiorina, LES of turbulent combustion: On the consistency between flame and flow filter scales, Proc. Combust. Inst. 35 (2) (2015) 1359–1366.
[30] W. Meier, P. Weigand, X. Duan, R. Giezendanner-Thoben, Detailed characterization of the dynamics of thermoacoustic pulsations in a lean premixed swirl flame, Combust. Flame 150 (1–2) (2007) 2–26.
[31] K. Bray, J.-B. Moss, A unified statistical model of the premixed turbulent flame, Acta Astronaut. 4 (1977) 291–319.
[32] N. Peters, Turbulent combustion, Cambridge University Press, 2000.
[33] P. Auzillon, B. Fiorina, R. Vicquelin, N. Darabiha, O. Gicquel, D. Veynante, Modeling chemical flame structure and combustion dynamics in LES, Proc. Combust. Inst. 33 (1) (2011) 1331–1338.
[34] M. Boger, D. Veynante, H. Boughanem, A. Trouvé, Direct numerical simulation analysis of flame surface density concept for large eddy simulation of turbulent premixed combustion, Symp. (Int.) Combust. 27 (1998) 917–925.
[35] K. Bray, M. Champion, P. Libby, The interaction between turbulence and chemistry in premixed turbulent flames, in: R. Borghi, S. Murphy (Eds.), Turbulent Reacting Flows, Lecture Notes in Engineering, 40, Springer (1989), pp. 541–563.
[36] T. Chew, R. Britter, K. Bray, Laser tomography of turbulent premixed bunsen flames, Combust. Flame 75 (2) (1989) 165–174.
[37] J. Galpin, A. Naudin, L. Vervisch, C. Angelberger, O. Colin, P. Domingo, Large-eddy simulation of a fuel-lean premixed turbulent swirl-burnel, Combust. Flame 155 (2008) 247–266.
[38] P. Domingo, L. Vervisch, D. Veynante, Large-eddy simulation of a lifted methane jet flame in a vitiated coflow, Combust. Flame 152 (2008) 415–432.
[39] M.S. Sweeney, S. Hochgreb, M.J. Dunn, R.S. Barlow, A comparative analysis of flame surface density metrics in premixed and stratified flames, Proc. Combust. Inst. 33 (1) (2011) 1419–1427.
[40] M.S. Sweeney, S. Hochgreb, M.J. Dunn, R.S. Barlow, The structure of turbulent stratified and premixed methane/air flames I: non-swirling flows, Combust. Flame 159 (9) (2012a) 2896–2911.
[41] M.S. Sweeney, S. Hochgreb, M.J. Dunn, R.S. Barlow, The structure of turbulent stratified and premixed methane/air flames II: Swirling flows, Combust. Flame 159 (9) (2012b) 2912–2929.
[42] R. Zhou, S. Balusamy, M.S. Sweeney, R.S. Barlow, S. Hochgreb, Flow field measurements of a series of turbulent premixed and stratified methane/air flames, Combust. Flame 160 (10) (2013) 2017–2028.
[43] M.S. Sweeney, S. Hochgreb, M.J. Dunn, R.S. Barlow, Multiply conditioned analyses of stratification in highly swirling methane/air flames, Combust. Flame 160 (2) (2013) 322–334.
[44] M. Euler, R. Zhou, S. Hochgreb, A. Dreizler, Temperature measurements of the bluff body surface of a swirl burner using phosphor thermometry, Combust. Flame 161 (11) (2014) 2842–2848.
[45] R.S. Barlow, M.J. Dunn, M.S. Sweeney, S. Hochgreb, Effects of preferential transport in turbulent bluff-body-stabilized lean premixed CH4/air flames, Combust. Flame 159 (8) (2012) 2563–2575.
[46] M.M. Kamal, R.S. Barlow, S. Hochgreb, Conditional analysis of turbulent premixed and stratified flames on local equivalence ratio and progress of reaction, Combust. Flame 162 (10) (2015) 3896–3913.
[47] M.M. Kamal, R.S. Barlow, S. Hochgreb, Scalar structure of turbulent stratified swirl flames conditioned on local equivalence ratio, Combust. Flame 166 (2016) 76–79.
[48] V. Katta, W.M. Roquemore, C/H atom ratio in recirculation-zone-supported premixed and nonpremixed flames, Proc. Combust. Inst. 34 (1) (2013) 1101–1108.
[49] F. Proch, A.M. Kempf, Numerical analysis of the cambridge stratified flame series using artificial thickened flame LES with tabulated premixed flame chemistry, Combust. Flame 161 (10) (2014) 2627–2646.
[50] S. Nambully, P. Domingo, V. Moureau, L. Vervisch, A filtered-laminar-flame PDF sub-grid scale closure for LES of premixed turbulent flames. part I: formalism and application to a bluff-body burner with differential diffusion, Combust. Flame 161 (7) (2014a) 1756–1774.
[51] S. Nambully, P. Domingo, V. Moureau, L. Vervisch, A filtered-laminar-flame PDF sub-grid-scale closure for LES of premixed turbulent flames. part II: application to a stratified bluff-body burner, Combust. Flame 161 (7) (2014b) 1775–1791.
[52] R. Mercier, T. Schmitt, D. Veynante, B. Fiorina, The influence of combustion SGS submodels on the resolved flame propagation. application to the LES of the cambridge stratified flames, Proc. Combust. Inst. 35 (2) (2015) 1259–1267.
[53] F. Proch, P. Domingo, L. Vervisch, A.M. Kempf, Flame resolved simulation of a turbulent premixed bluff-body burner experiment. part I: analysis of the reaction zone dynamics with tabulated chemistry, Combust. Flame 180 (2017a) 321–339.
[54] F. Proch, P. Domingo, L. Vervisch, A.M. Kempf, Flame resolved simulation of a turbulent premixed bluff-body burner experiment. part II: a-priori and a–posteriori investigation of sub-grid scale wrinkling closures in the context of artificially thickened flame modeling, Combust. Flame 180 (2017b) 340–350.
[55] T. Brauner, W.P. Jones, A.J. Marquis, LES of the cambridge stratified swirl burner using a sub-grid PDF approach, Flow Turbul. Combust. 96 (4) (2016) 965–985.
[56] V. Moureau, P. Domingo, L. Vervisch, Design of a massively parallel CFD code for complex geometries, Comptes Rendus Mécanique 339 (2–3) (2011) 141–148.
[57] F. Charlette, C. Meneveau, D. Veynante, A power-law flame wrinkling model for LES of premixed turbulent combustion, part ii: dynamic formulation, Combust. Flame 131 (2/2) (2002) 181–197.
[58] D. Veynante, V. Moureau, Analysis of dynamic models for large eddy simulations of turbulent premixed combustion, Combust. Flame 162 (12) (2015) 4622–4642.
[59] D. Veynante, R. Knikker, Comparison between LES results and experimental data in reacting flows, J. Turbul. 7 (35) (2006) 1–20.
[60] P. Nilsson, X. Bai, Effects of flame stretch and wrinkling on co formation in turbulent premixed combustion, Proc. Combust. Inst. 29 (2) (2002) 1873–1879.